PNNL-14144

Pacific Northwest
National Laboratory
Operated by Battelle for the
U.S. Department of Energy

Retrieval and Pipeline Transfer Assessment of Hanford Tank 241-AN-105 Waste

Y. Onishi
J.M. Tingey
B.E. Wells
J. Lui
G. Terrones
K.P. Recknagle
S.T. Yokuda
M. Quinn

January 2003

Prepared for the U.S. Department of Energy
under Contract DE-AC06-76RL01830

DISCLAIMER

PACIFIC NORTHWEST NATIONAL LABORATORY
operated by
BATTELLE
for the
UNITED STATES DEPARTMENT OF ENERGY
under Contract DE-AC06-76RL01830

Printed in the United States of America
Available to DOE and DOE contractors from the
Office of Scientific and Technical Information,
P.O. Box 62, Oak Ridge, TN 37831-0062;
ph: (865) 576-8401
fax: (865) 576-5728
email: reports@adonis.osti.gov
Available to the public from the National Technical Information Service,
U.S. Department of Commerce, 5285 Port Royal Rd., Springfield, VA 22161
ph: (800) 553-6847
fax: (703) 605-6900
email: orders@ntis.fedworld.gov
online ordering: http://www.ntis.gov/ordering.htm

 This document was printed on recycled paper.
(8/00)

PNNL-14144

Retrieval and Pipeline Transfer Assessment of Hanford Tank 241-AN-105 Waste

Y. Onishi
J. M. Tingey
B. E. Wells
J. Lui
G. Terrones
KP Recknagle
S. T. Yokuda
M. Quinn

January 2003

Prepared for
the U.S. Department of Energy
under Contract DE-AC06-76RLO 1830

Pacific Northwest National Laboratory
Richland, WA 99352

Summary

In this study Pacific Northwest National Laboratory (PNNL) assessed the following five steps for Hanford Tank 241-AN-105 waste retrieval and subsequent pipeline transfer:

Step 1. Remove supernatant liquid waste from AN-105 and transfer it through a pipeline with inline dilution with water (1st liquid waste transfer).
Step 2. Add water (as a diluent) to Tank AN-105.
Step 3. Mix the saltcake waste and water with mixer pumps to dissolve soluble solids.
Step 4. Let undissolved solids settle to the tank bottom.
Step 5. Remove the resulting supernatant liquid waste from Tank AN-105 (2nd liquid waste transfer).

To assess these five steps of waste retrieval and slurry pipeline transfer, AN-105 waste rheology measurements were conducted and solids identified with bright field image (BF), select area diffraction (SAD), and energy dispersive x-ray spectroscopy (EDS). By combining available in situ and laboratory data, PNNL developed the AN-105 specific viscosity model, changing from several centipoise of viscosity to tens of millions of centipoise as a function of strain rate and solid concentration. This viscosity model was implemented to the TEMPEST code used to simulate AN-105 pump jet mixing.

For the first waste transfer (Waste Retrieval Step 1), the AN-105 supernatant liquid would be diluted by water at a ratio of 1 volume liquid waste to 0.56 volume water. Chemical modeling indicates that 56 vol% dilution of the AN-105 supernatant liquid with water may precipitate small amounts of $Al(OH)_3(s)$ and $Cr(OH)_3(s)$. However, the BF, EDS, and SAD measurements of AN-105 saltcake did not detect gibbsite [$Al(OH)_3(s)$]. Thus, in spite of the chemical model's prediction of gibbsite, it is possible that gibbsite would not precipitate under this inline dilution condition. Assuming that gibbsite does precipitate, we estimated that the critical velocity of this diluted AN-105 waste would be approximately 0.3 m/s (1 ft/sec) to maintain turbulent flow. Thus, there would be no solid deposition in the pipeline when the expected slurry pipeline velocity is about 1.2–1.8 m/s (4–6 ft/sec). These evaluations indicate that inline dilution of AN-105 supernatant liquid waste with water would have no adverse impact on AN-105 supernatant liquid properties that would hinder waste pipeline transfer.

After confirming the reasonableness of our chemical model predictions with AN-105 experimental dilution data, we simulated chemical reactions due to saltcake dilution by water (Steps 2 and 3). The AN-105 dilution model predicts that all $Na_2CO_3 \cdot H_2O(s)$ and $Na_2SO_4(s)$ would be dissolved. This would reduce the saltcake waste volume by over 90%. The remaining solids [$Cr(OH)_3(am)$, $Ca(OH)_2(s)$, and possibly $Na_2C_2O_4(s)$] are expected to settle easily (Step 4), and would be separated from the supernatant liquid. Thus, it is very feasible to retrieve the resulting supernatant liquid from 79% in-tank dilution of the saltcake from AN-105 and to transfer the liquid waste through a 3-inch (0.07-m) pipeline (Waste Retrieval Step 5).

For assessing Waste Retrieval Step 3, we used the TEMPEST computer code to simulate mixing of AN-105 saltcake with water at a ratio of 1 volume of saltcake to 0.79 volume of water

by two mixer pumps under conservative conditions. The model predicted that after 30 minutes of mixing, the 20-ft, off-center, 300-hp mixer pumps would mobilize all the solids. The solids would be fully mixed over the entire tank even under the very conservative conditions imposed in this evaluation.

We also evaluated solid-liquid waste slurry transfer from Hanford Tank AN-105 to the AP Tank Farm. We selected seven cases comprising AN-105 fully mixed waste and fully mixed waste with 25, 50, and 100% dilution by water with and without accounting for solids dissolution. For all seven cases, critical velocities were estimated to be between 1.33 ft/sec (0.41 m/s) and 1.55 ft/sec (0.47 m/s), and associated pressure drops are 10 to 23 psi. At 4.9 ft/sec (0.71 m/s) and 6 ft/sec (1.8 m/s) velocities, the pressure drops for waste without dilution are 178 and 252 psi, respectively. The waste with dilution requires less pressure drop. All the pressure drops are less than the maximum available system pressure head of 275 psi. Thus AN-105 waste can be transferred to the AP Tank Farm through the existing 3-inch pipeline system at these velocities.

This Tank AN-105 waste retrieval assessment concludes that the AN-105 liquid waste can be retrieved with inline and in-tank dilution. Two 300-hp mixer pumps would erode all AN-105 saltcake and distribute it uniformly throughout the entire tank. The AN-105 slurry waste can also be transferred through a 3-inch (0.07-m) pipeline to Tanks AP-102 and AP-104 under the waste and mixing conditions used in this assessment.

Contents

Figures

Tables

1.0 Introduction

The objective of the study was to assess waste retrieval and subsequent pipeline transfer for Hanford Tank 241-AN-105. The tank is located in the AN Tank Farm of the 200 East Area on the U.S. Department of Energy's (DOE) Hanford Site in southeastern Washington State. It is one of 28 double-shell tanks (DSTs). The tank went into service in 1982 and has received primarily double-shell slurry feed (DSSF) associated with evaporation campaigns. The most recent additions contained small volumes of flush water.

The tank currently contains 591,700 gallons (2,240 m^3) of supernatant liquid, 48,800 gallons (185 m^3) of crust, and 487,900 gallons (1,850 m^3) of saltcake radioactive waste (Wells et al. 2002). The main aqueous chemical species of the supernatant liquid [Na^+, CO_3^{2-}, SO_4^{2-}, OH^-, NO_3^-, $NaNO_3$(aq), NO_2^-, $NaNO_2$(aq), $Al(OH)_4^-$, Cl^-, $Cr(OH)_4^-$, $H_2SiO_4^{2-}$] are in equilibrium condition with solids mainly consisting of $NaCO_3 \cdot H_2O$(s), $NaSO_4$(s), $Cr(OH)_3$(s), and $Ca(OH)_3$ in saltcake form.

The following five steps describe the baseline retrieval process for AN-105 waste (Orme et al. 2001):

Step 1. Remove supernatant liquid waste from AN-105 and transfer it through a pipeline with inline dilution with water (1st liquid waste transfer).
Step 2. Add water (as a diluent) to Tank AN-105.
Step 3. Mix the saltcake waste and water with mixer pumps to dissolve soluble solids within the tank.
Step 4. Let undissolved solids settle to the tank bottom.
Step 5. Remove the resulting supernatant liquid waste from Tank AN-105 (2nd liquid waste transfer).

To assess the waste retrieval and pipeline transfer, we evaluated the following:

For Step 1:

- Chemical reactions of inline dilution of AN-105 supernatant liquid with water
- Feasibility of the diluted liquid waste pipeline transfer (1st liquid waste transfer)

For Steps 2 and 3:

- Chemical reactions of in-tank dilution of AN-105 saltcake with water
- Effectiveness of two 300-hp pumps to mix the AN-105 saltcake and water

Step 4:

- Ability of remaining solids to settle

Step 5:

- Feasibility of the diluted liquid waste pipeline transfer (2nd liquid waste transfer).

The feasibility of transferring diluted AN-105 slurry (a mixture of solids and liquid waste with and without dilution with water) through a 3-inch pipeline to Tanks 241-AP-102 and 241-AP-104 was also evaluated. PNNL had previously determined that if the AN-105 slurry diluted by 25 and 180 vol% with water were placed in Tanks AP-102 and AP-104, single 300-hp pumps in the centers of those receiver tanks would suspend and uniformly mix all the solids (Onishi and Recknagle 1998).

To perform the evaluations listed above, PNNL conducted

- AN-105 rheology measurements
- Identification of AN-105 solids by bright field image (BF), select area diffraction (SAD), and energy dispersive x-ray spectroscopy (EDS)
- Chemical modeling with the GMIN code (Felmy 1995)
- Pump jet mixing with the TEMPEST code (Trent and Eyler 1993; Onishi and Trent 1999)
- Slurry pipeline transport modeling.

Section 2 describes previously available AN-105 rheology data, our rheology experimental results, and solid characterization. Predicted chemical reactions for inline and in-tank dilution processes are presented in Section 3. Section 3 also discusses the feasibility of the 1st and 2nd liquid waste transfers through the pipeline and the ability of the solids to settle in Tank AN-105. The assessment of mixing the saltcake and water with a pump jet is discussed in Section 4. Section 5 presents the assessment of pipeline transfer of the diluted AN-105 slurry. The summary and conclusions are stated in Section 6, while cited references are listed in Section 7. In addition, Appendix A presents crystallinity, morphology, chemical composition, and crystal phases of AN-105 saltcake obtained by BF, SAD, and EDS measurements. Appendix B discusses the slurry pipeline transfer assessment methodologies.

2.0 AN-105 Tank Waste Characteristics

2.1 Tank Waste and Its Retrieval

Tank AN-105 is one of 28 DSTs at Hanford. It is an active tank that has received primarily double-shell slurry feed (DSSF) from 1982 to the present. The tank has a diameter and operating depth of 75 ft (23 m) and 35 ft (10.7 m), respectively. Its operational storage capacity is 1,160,000 gallons (4,390 m^3). The tank contains radioactive waste comprising 591,700 gal (2,240 m^3) of supernatant liquid, 48,800 gal (185 m^3) of crust, and 487,900 gal (1,850 m^3) of saltcake (Wells et al. 2002). The supernatant liquid and crust occupy 233 in. (5.91 m), and the saltcake occupies 177 in. (4.5 m) of the total waste depth of 410 in. (10.41 m). These depths correspond to 56.8 vol% supernatant liquid and crust and 43.2 vol% saltcake. The waste temperature is between 32° and 43°C.

The density of the supernatant liquid is 1,430 kg/m^3. Its viscosity is approximately 4 cP (Herting 1997). The saltcake density is 1,580 kg/m^3 (Wells et al. 2002). The saltcake has an average yield strength of approximately 150 Pa (Stewart et al. 1996). The rheology of the AN-105 waste is discussed in detail in Section 2.3.

The dry solid density is estimated to be 2,230 kg/m^3 based on solids composition and water content in the liquid and saltcake (see Onishi et al. 2002), resulting in a solid volume fraction of approximately 19%. Solid particle diameters vary from 0.5 to 70 μm with a median size of 5.8 μm, as shown in Figure 2.1 (Herting 1997**)**. The current AN-105 model divided solids into four groups by size. The percent by weight (which is the same as volume percent in this case) of these four size fractions are listed in Table 2.1.

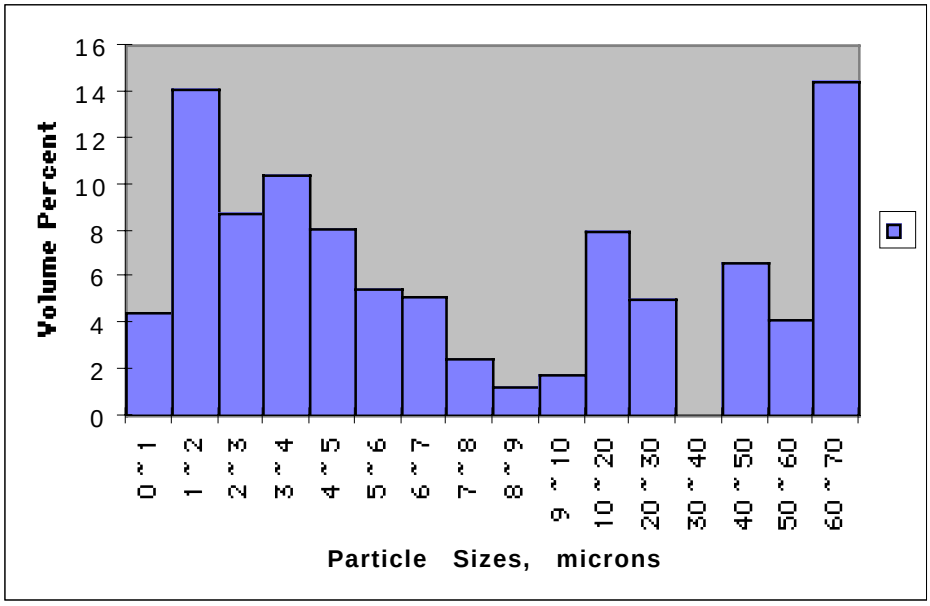

Figure 2.1. Particle Size Distribution of AN-105 Waste (Herting 1997)

Table 2.1. Four Particle Sizes Used in the Current AN-105 Model

	Solid 1	Solid 2	Solid 3	Solid 4
Size, μm	0.5–3	3–10	10–30	40–70
Amount in Saltcake, wt%	27.4	34.3	13.0	25.3

As indicated in Section 1, the AN-105 waste retrieval process is expected to consist of the following five steps (Orme et al. 2001):

Step 1. Remove supernatant liquid waste from AN-105 and transfer it through a pipeline with inline dilution with water (assigned at 1 volume of AN-105 liquid waste to 0.56 volume of water in this study).
Step 2. Add water (as a diluent) to AN-105 (assigned at 1 volume of AN-105 saltcake to 0.79 volume of water in this study).
Step 3. Mix the saltcake waste and water with mixer pumps to dissolve soluble solids.
Step 4. Let undissolved solids settle to the tank bottom.
Step 5. Remove the resulting supernatant liquid waste from AN-105.

To perform Step 3, two 300-hp mixer pumps would be installed 20 ft (6.1 m) off-center in AN-105 to mix the saltcake with water and dissolve much of solids (see Figure 2.2). (After this study was conducted, mixer pumps were redesigned to have the pump injection nozzle moved from the top of the pump to the bottom [Onishi et al. 2002].)

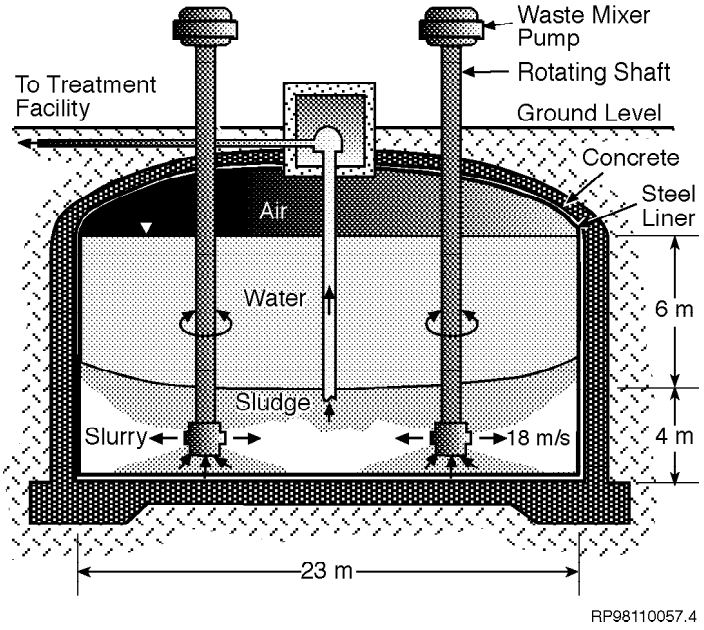

Figure 2.2. Tank Waste Mixing Setup

2.2 AN-105 Waste Rheology

2.2.1 Previously Measured AN-105 Rheology

Two sets of rheology data were available prior to undertaking this study. They are in situ measurements (Stewart et al. 1996) and laboratory measurements (Herting 1997). Figure 2.3 shows the vertical distribution of the in situ yield strength (stress) of the AN-105 saltcake measured by the first pass of the ball rheometer. This figure shows that the yield strength increased with depth varying from 40 Pa near the surface of the saltcake to 185 Pa at about 20 cm above the tank bottom.

As indicated in Section 2.1, Step 3 of the AN-105 baseline waste retrieval process is to mix the saltcake waste and water with mixer pumps to dissolve soluble solids. Under Step 3, most soluble AN-105 solids would be dissolved, as discussed in Section 3, and the action of the mixer pumps would disturb the waste.

To determine the yield stress of the disturbed waste, we reevaluated the ball rheometer data. Multiple passes of the ball rheometer were made through the saltcake. We used calculations that were more precise than the original 1996 calculations and a correction for the actual ball speed during measurements to obtain more accurate estimates. As shown in Figures 2.4 and 2.5, yield strength became less as the ball rheometer repeatedly passed through the AN-105 saltcake.

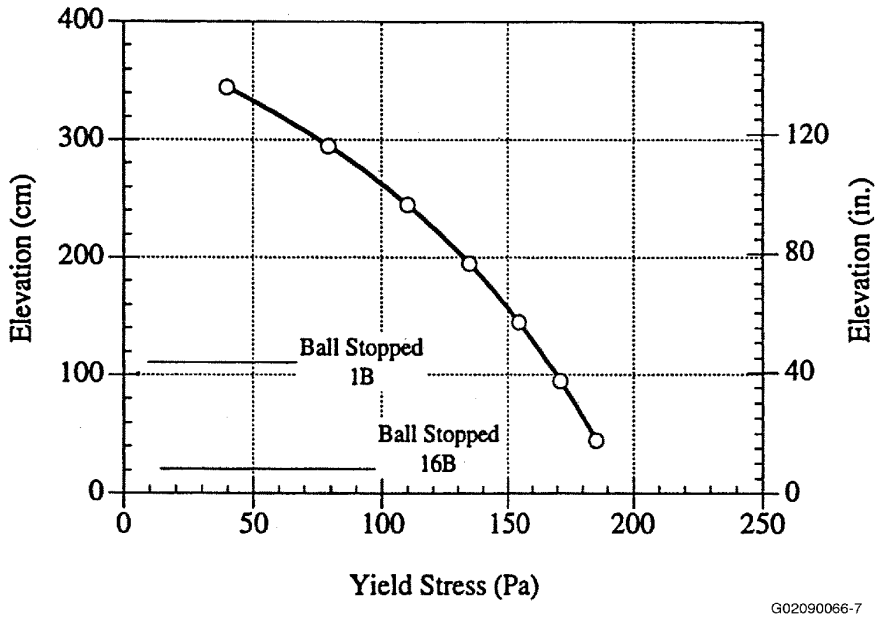

Figure 2.3. AN-105 Yield Strength Measured by First Pass of the Ball Rheometer (Stewart et al. 1996)

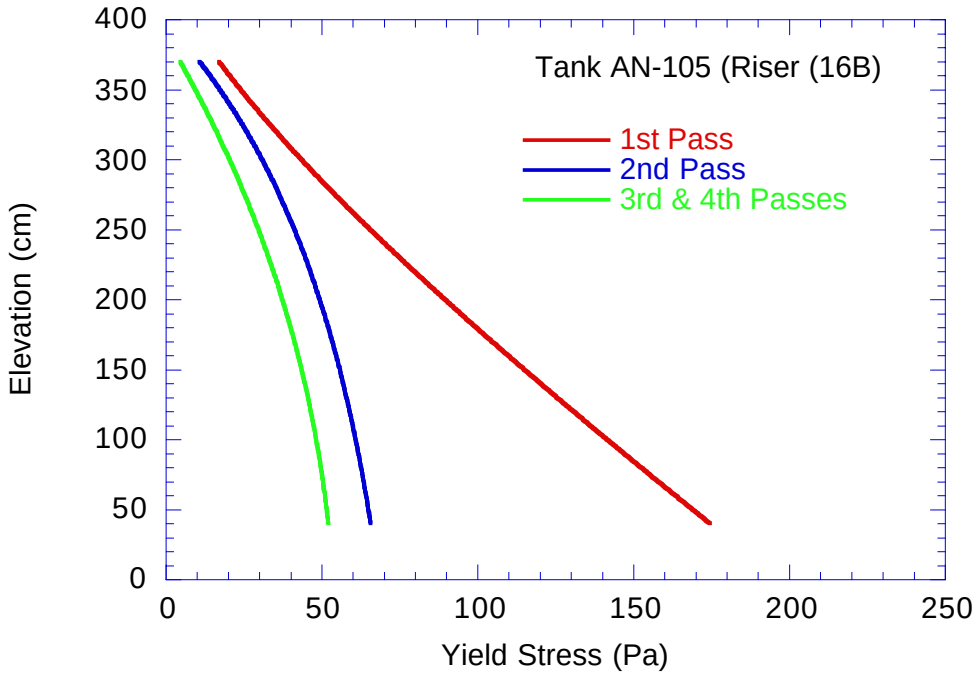

Figure 2.4. In Situ Yield Strength of AN-105 Waste Measured at Riser 16B

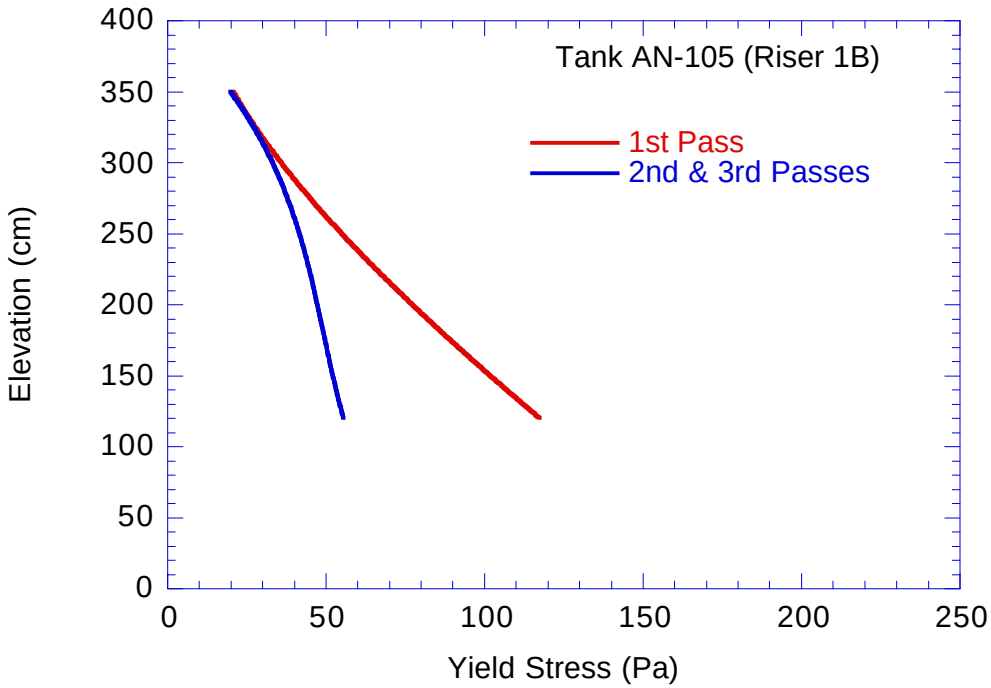

Figure 2.5. In Situ Yield Strength of AN-105 Waste Measured at Riser 1B

The time elapsed between each measurement at a given elevation was estimated to be at least 50 minutes. The results shown in these figures indicate that the yield strength is sensitive to shear history and approaches an asymptotic limit with several repeated shearings.

At riser 16B (Figure 2.4), the measured maximum yield strength was reduced from 170 Pa on the first pass to 50 Pa on the fourth pass. Data for the third and fourth passes in riser 16B were almost equivalent (the standard deviations overlapped). Therefore, these two passes were combined. At riser (1B) (Figure 2.5), the yield strength was reduced from 120 Pa on the first pass to 55 Pa on the second and third pass. These measurements suggest that the yield strength would be reduced to a maximum of 55 Pa (roughly one-third reduction from the strength of the undisturbed waste), once the AN-105 saltcake was disturbed. It is interesting to note that the disturbed sludge (not saltcake) waste in Tank 241-AZ-102 has a yield strength of 60 Pa, while the undisturbed AZ-102 sludge has a yield strength of 1,540 Pa.[(a)]

There are also in situ yield strength measurements on AN-104 waste (Stewart et al. 1996). Because AN-104 and AN-105 wastes are physically and chemically similar (Herting 1997, 1998), we also determined AN-104 waste's yield strength for multiple passes of the ball rheometer. As expected, AN-104 yield strength and changes with subsequent passes are similar to those of AN-105. Figure 2.6 shows the average vertical distribution of yield strength based on the final passes of the ball rheometer at risers 16B and 1B in Tanks AN-104 and AN-105. As indicated in this figure, the average yield strength of disturbed AN-104 and AN-105 waste varied from 5 Pa near the saltcake surface to 62 Pa just above the tank bottoms.

In situ viscosity distributions of the AN-105 saltcake measured by a ball rheometer moving at 0.1, 1, and 10 cm/s (or at strain rates of 0.01, 0.1 and 1.0 s^{-1}) on the first and last passes are shown in Figure 2.7 (Stewart et al. 1996). This figure indicates very high saltcake viscosity values, ranging from $2x10^4$ to $2x10^7$ cP, depending on the strain rates. Similar to yield strength, repeated ball rheometer measurements reduced the saltcake viscosity by two to five times.

Herting (1997) measured AN-105 rheology at the Hanford 222-S Laboratory. He conducted measurements of four AN-105 samples: 1) whole-tank composite (WTC) having the same saltcake to supernatant liquid volume ratio as the fully mixed tank, 2) WTC diluted by water at a ratio of 1 volume WTC to 0.5 volume water, 3) saltcake alone, and 4) saltcake diluted by water at a ratio of 1 volume saltcake to 0.8 volume water. Each sample was tested at three temperatures. Figure 2.8 shows the measured shear stress of the saltcake sample as a function of the strain rate at the in situ saltcake temperature of approximately 40°C, showing yield strength of 0.5 Pa or less (see the value of the shear stress at zero strain rate). Figure 2.9 shows the measured viscosity variation with strain rate in the saltcake sample at the same temperature. Two lines in each figure exhibit data obtained in ascending and descending orders of strain rate between 1.5 and 300 s^{-1}, showing no hysteresis. These measurements indicate that the maximum viscosity is approximately 360 cP at a strain rate of 1.5 s^{-1}. Herting's measurements also indicate that viscosity is constant (about 25 cP) at a strain rate above 100 s^{-1}. Similar behavior was also

(a) Gray WJ, ME Peterson, RD Scheele, and JM Tingey. 1993. *Characterization of the First Core Sample of Neutralized Current Acid Waste from Double-Shell Tank 241-AZ-102.* Unpublished report, Pacific Northwest National Laboratory, Richland, WA.

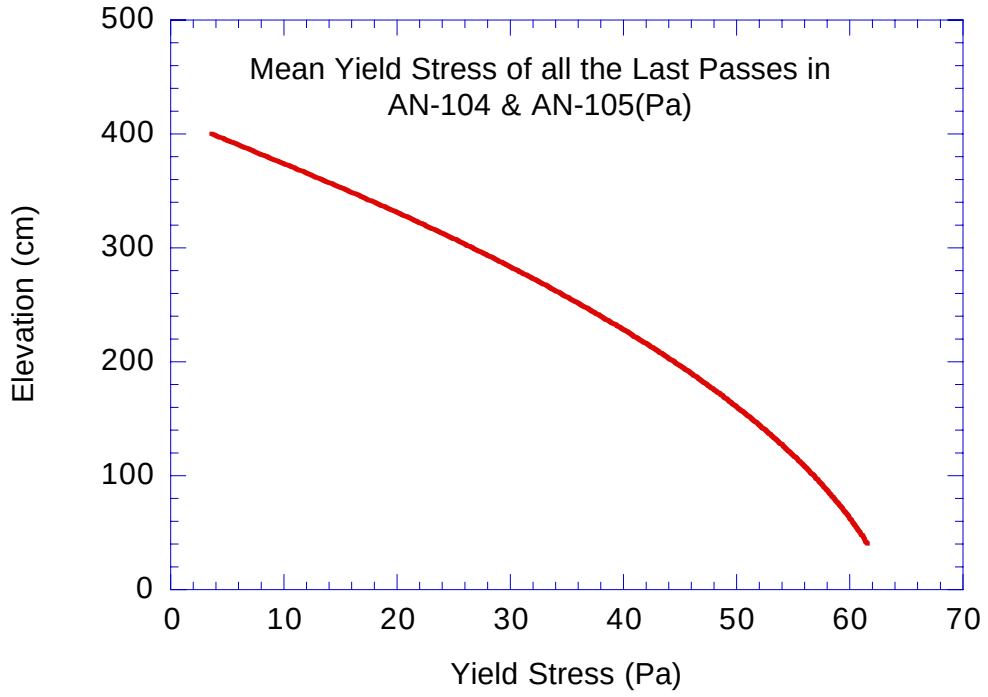

Figure 2.6. Average In Situ Yield Stress of AN-104 and AN-105 Wastes on Final Passes of the Ball Rheometer

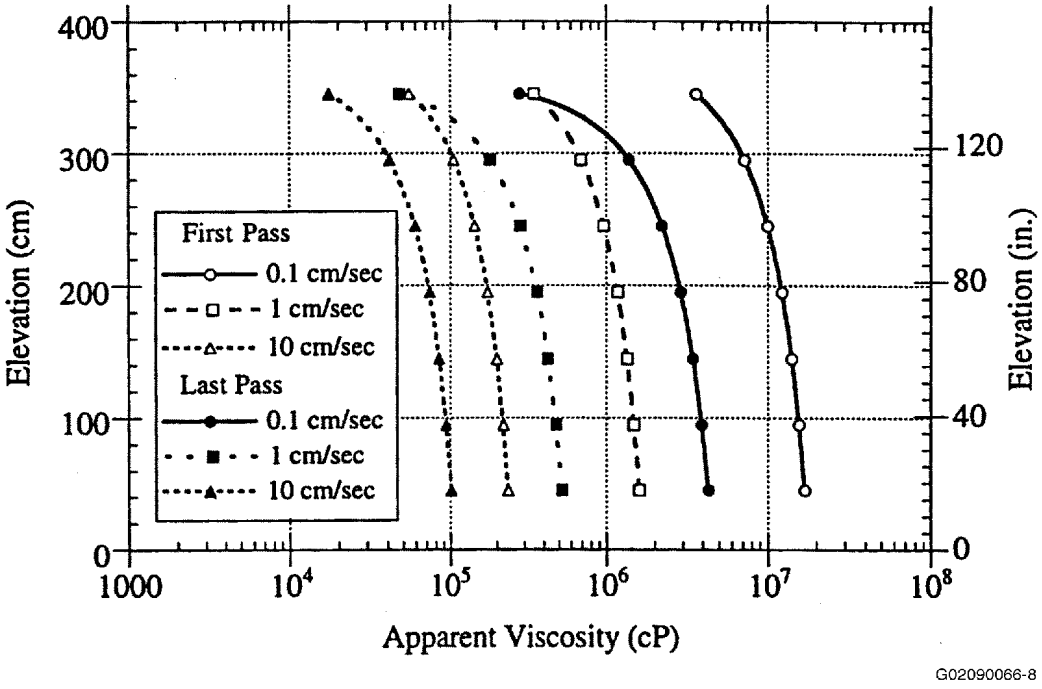

Figure 2.7. Saltcake Viscosity Distributions on the First and Last Passes (Stewart et al. 1996)

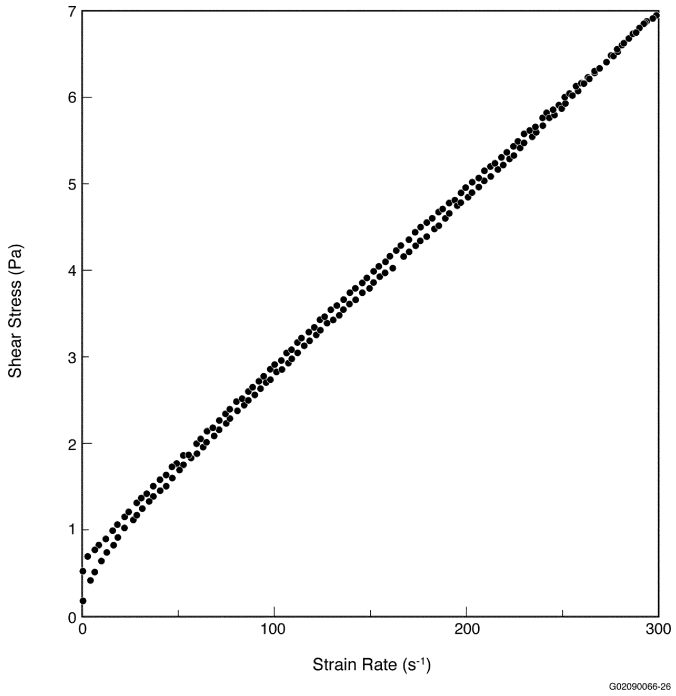

Figure 2.8. Shear Stress Versus Strain Rate of AN-105 Saltcake (Herting 1997)

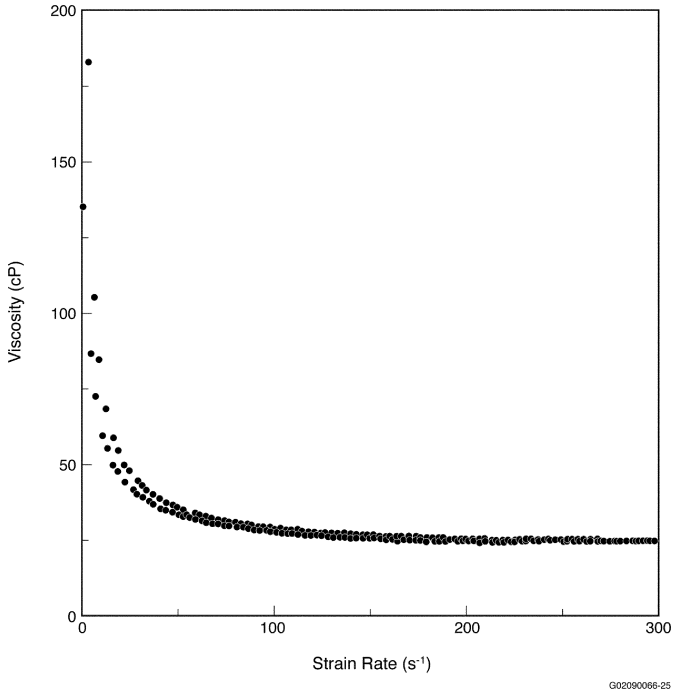

Figure 2.9. Viscosity Versus Strain Rate of AN-105 Saltcake (Herting 1997)

observed at 25° and 65°C. Herting stated that the rheometer was not reliable when the strain rate was below 30 s^{-1}. These measured values of yield strength and viscosity are greatly different from in situ measurements shown in Figures 2.4 and 2.5. Note that the viscosity reported by Herting (1997) is the *apparent* viscosity. The apparent viscosity is calculated by dividing the shear stress by its associated strain rate. To reconcile these differences we conducted the AN-105 rheology measurements that are presented in Section 2.2.2.

2.2.2 AN-105 Rheology Measurements

PNNL received six samples of AN-105 waste material from a Hanford contractor for physical and rheological characterization. These samples included four samples from core #152 and two samples from core #153. A list of the sample numbers and their corresponding core and segments are given in Table 2.2.

Tank AN-105 contains primarily double-shell slurry feed (DSSF) as described in Section 2.1. Cores 152 and 153 were taken from risers 12A and 7B, respectively, during June of 1996. A total of 22 segments in each core were obtained from this tank. Two small subsamples (a total of 3 grams) were taken from each of these samples, and the remaining sample was composited. Water was added to the composite to correct for water lost during storage of these samples. The mass of each sample and the mass of water added to the composite are reported in Table 2.3.

Table 2.2. Sample Numbers

Core #	Segment	Subsegment
152	16	Upper Half
	18	Upper Half
	20	Lower Half
	22	Composite
153	15	Lower Half
	22	Upper Half

Table 2.3. Composite Inventory

Sample (Core/Segment)	Mass (g)	
	Sample	Water
152/16	63.02	0.00
152/18	15.95	4.15
152/20	54.55	0.0
152/22	54.37	2.18
153/15	88.44	14.15
152/22	59.60	7.75

Three dilutions were made from subsamples of this composite. The dilutions were prepared by adding supernatant, inhibited water (2 M NaOH), or both. The amounts of each component in these dilutions are given in Table 2.4. The densities of the composite, supernatant, and inhibited water are 1.58, 1.247, and 1.080 g/mL, respectively. The volume percent of the composite in each of these dilutions is 42% for the supernatant dilution, 50% for the water dilution, and 28.2% for the supernatant and water dilution.

Table 2.4. Dilution Preparation

Dilution	Mass (g)		
	Composite	**Supernatant**	**Inhibited Water**
Supernatant	101.95	110.89	0.00
Water	101.59	0.00	69.42
Supernatant/Water	51.05	54.80	41.31

Rheological characterization was performed in duplicate on each of the dilutions, the composite, and the settled supernatant from the supernatant dilution. The rheological properties of these samples were measured at 25°C. Rheological measurements included shear stress as a function of shear rate. From these measurements the viscosity of the sample as a function of shear rate and the yield stress can be calculated.

Experimental

The shear stress of the sample as a function of shear rate was determined using a Bohlin CS rheometer with a C25 geometry. Calibration checks were made with certified 50- and 10-cP viscosity standards to ensure that the viscometer was operating properly. The sample was transferred to the rheometer cup and controlled at the desired temperature with a constant-temperature bath. The shear rate was gradually ramped from 0 to 350 rps, and the shear stress was recorded as function of shear rate. The (apparent) viscosity was then calculated by dividing the shear stress by the shear rate. The yield stress was also obtained from this measurement.

A rheogram for a material with a yield stress has two parts. The first portion appears as a nearly vertical line beginning at the origin and running up the ordinate. This portion of the rheogram records the behavior of the material as it acts like a solid or gel. When sufficient force is transmitted to the material to break the gel or make it yield, the rheogram will angle sharply to the right, and from then on the behavior of the material is recorded as a fluid. The point in the curve at which the sample transfers from a solid or gel to a fluid is the yield point. The stress at this point measured in Pascals on the ordinate is the value of the yield stress (strength).

Duplicate samples were measured on the composite, supernatant dilution, water dilution, and supernatant and water dilution. Some measurements were repeated on the same sample after allowing the sample to sit in the viscometer to determine the effect of shear on the viscosity and yield stress. Duplicate rheograms of the settled supernatant from these dilutions were also obtained.

Results

In Figure 2.10 the shear stress of the AN-105 composite is plotted as a function of shear rate. All three measurements made on the composite are provided in this figure. Curves for increasing (up-curve) and decreasing (down-curve) shear rates are provided for each measurement. The composite exhibits pseudoplastic behavior with a yield stress of approximately 0.25 Pa. A hysteresis is observed in these measurements, indicating that the composite is thixotropic. The rheology data for both the up- and down-curves were fit to a yield power law model (Eq. 2.1). The fit parameters for each curve are provided in Table 2.5. The apparent viscosity (shear stress/shear rate) of the composite as a function of shear rate is provided in Figure 2.11.

$$\tau = \tau_0 + \beta\gamma^n \tag{2.1}$$

where

n = coefficient
β = coefficient
τ = shear stress
τ_0 = yield stress
γ = shear rate.

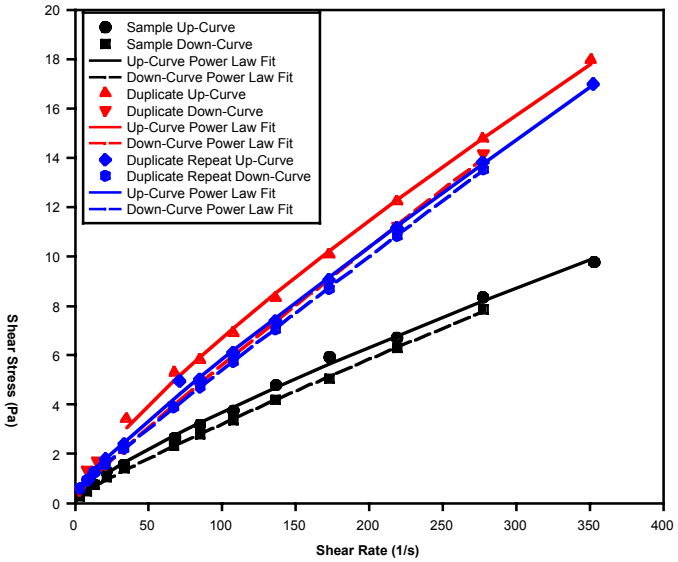

Figure 2.10. Rheograms for Sample and Duplicate Analysis of AN-105 Composite

The settled supernatant from the three dilutions exhibited Newtonian behavior. The viscosity of Newtonian liquids is independent of shear rate, as presented in Equation 2.2:

$$\tau = \mu\gamma \tag{2.2}$$

Table 2.5. Yield Power Law Model Parameters

Measurement	Curve	τ_0 (mPa)*	β (mPa)	n
Sample	Up	250	77.5	0.823
	Down	250	43.4	0.917
Duplicate	Up	350	153	0.808
	Down	350	69.5	0.939
Duplicate—Repeat	Up	540	81.2	0.906
	Down	540	57.2	0.964
* Not a fit parameter.				

where

τ = shear stress
μ = viscosity
γ = shear rate.

The viscosity of the settled solution from the water dilution (8 cP) was lower than the viscosity of the settled solution from the supernatant dilution (10 cP) even though the volume percent of the composite in the water dilution was slightly higher than in the supernatant dilution. This difference is probably due to the higher salt content in the settled solution than in the supernatant dilution. The water plus supernatant dilution contained a approximately half the volume percent composite as the other dilutions, resulting in a significantly lower viscosity for the settled liquid (5 cP). The viscosity of both the sample and duplicate for each of these solutions is reported in Table 2.6.

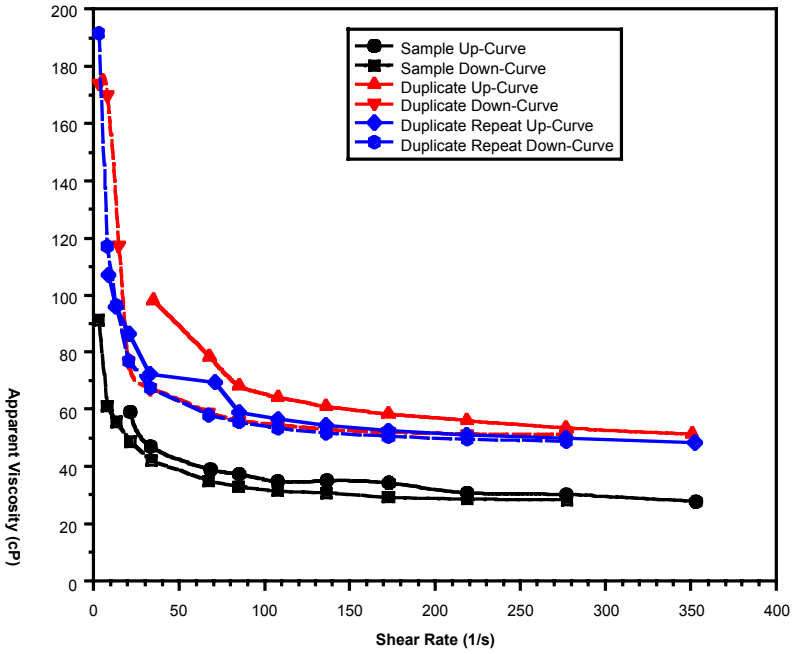

Figure 2.11. Apparent Viscosity as a Function of Shear Rate for the AN-105 Composite

Table 2.6. Viscosity of the Settled Supernatants from the AN-105 Composite Dilutions

Dilution	Measurement	Viscosity (cP)
Supernatant	Sample	10.3
	Duplicate	9.7
Water	Sample	8.3
	Duplicate	8.3
Supernatant + Water	Sample	4.5
	Duplicate	5.0

The up-curve on the first measurement made on the supernatant dilution indicated that the material had gel-like properties with a yield stress of 34.6 Pa. After the material yielded, the shear stress continued to drop with increasing shear rate. After the material yielded, it exhibited yield pseudoplastic behavior with a much lower yield stress (0.45 to 0.05 mPa). The initial behavior of this sample is shown in a plot of shear stress as a function of time (Figure 2.12). The duplicate sample did not display this same behavior but appears to exhibit Bingham plastic properties. Bingham plastics require a minimum amount of stress before deformation but then exhibit linear increases in shear stress as a function of shear rate. Bingham plastics are modeled by a function similar to the power law used to model the yield pseudoplastic materials except that the exponent (n) equals 1.0 (see Eq. 2.1). The fit parameters for each measurement of the supernatant dilutions except for the up-curve of the first run are provided in Table 2.7. A down-curve was not obtained on the second repeat analysis of the duplicate. The rheograms for all the supernatant dilution measurements are compared in Figure 2.13, and the apparent viscosity of these dilutions calculated from the rheograms is plotted as a function of shear rate in Figure 2.14.

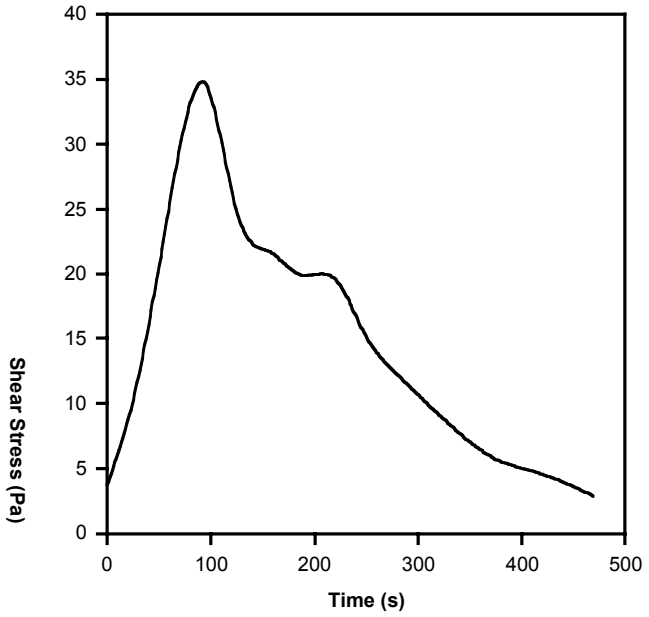

Figure 2.12. Yield Behavior of the Supernatant Dilution

Table 2.7. Supernatant Dilution Rheology Curve Fits

Measurement	Curve	τ_0 (mPa)[(a)]	β (mPa)	n
Sample	Down	53	20.2	0.863
Sample—Repeat	Up	119	11.8	1.000
	Down	71	13.1	0.986
Duplicate	Up	60	6.1	1.0
	Down	43	6.1	1.0
Duplicate—1st Repeat	Up	41	6.0	1.0
	Down	67	5.4	1.0
Duplicate—2nd Repeat	Up	31	6.6	1.0
(a) Not a fit parameter.				

Both the water dilution and supernatant plus water dilution exhibited Newtonian behavior with viscosities similar to those observed by the settled supernatants for these dilutions. The viscosities of each measurement of the water and supernatant plus water are reported in Table 2.8. The solids in these dilutions settle quickly, making it difficult to obtain accurate viscosities of the suspended solutions and may have contributed to measuring viscosities similar to those obtained for the settled liquid.

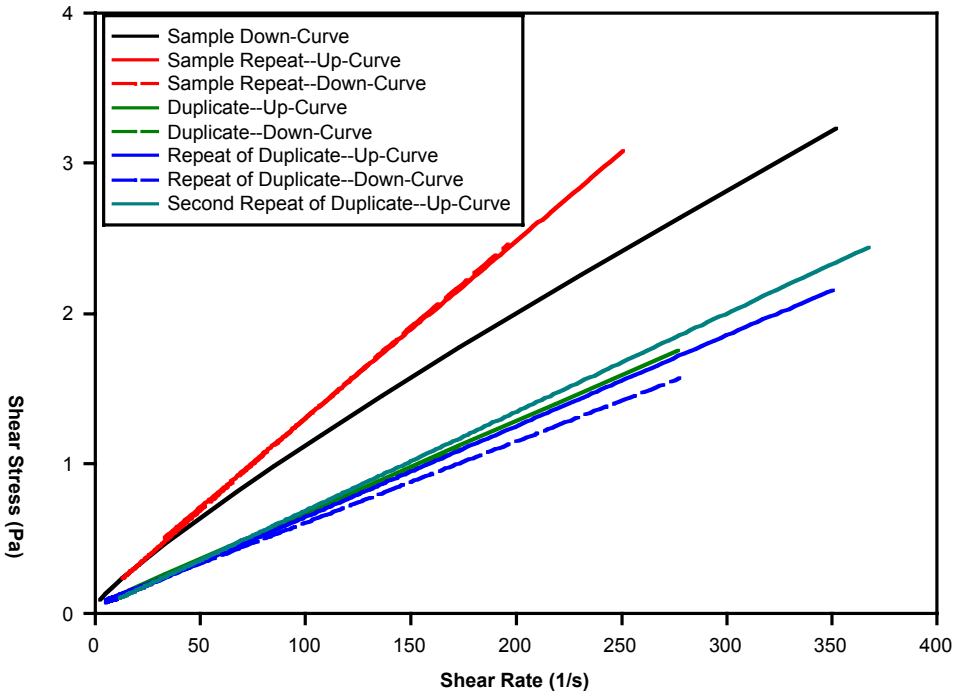

Figure 2.13. Comparison of Rheograms of Sample and Duplicate of the Supernatant Dilutions

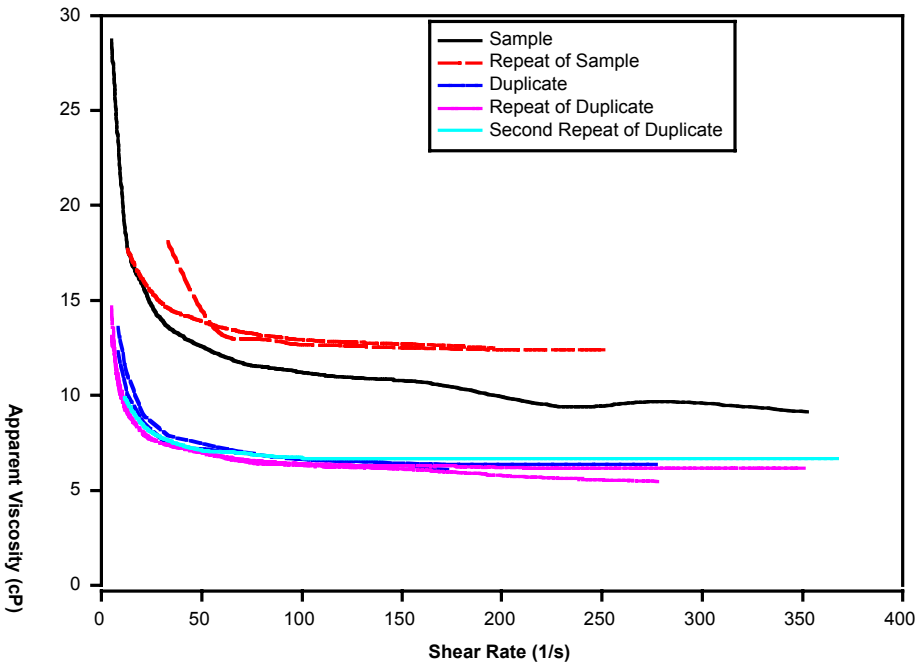

Figure 2.14. Apparent Viscosity as a Function of Shear Rate for the Supernatant Dilutions

Table 2.8. Viscosity of the Water and Water Plus Supernatant Dilutions

Dilution	Measurement	Viscosity (cP)
Water	Sample	7.4
	Sample-Repeat	8.4
	Duplicate	7.2
Supernatant + Water	Sample	4.3
	Sample-Repeat	4.8
	Duplicate	4.0

2.2.3 Waste Viscosity Equation

The viscosity of AN-105 waste varies from approximately 4 cP in the supernatant liquid to 2 x 10^7 to 20 cP in the saltcake, as presented in Sections 2.1, 2.2.1, and 2.2.2. Thus, AN-105 waste is non-Newtonian when strain rate is small and the solid concentration is high. The waste also displays time-varying behavior (i.e., thixotropic). When it is diluted or subject to a high strain rate, AN-105 waste exhibit a Newtonian behavior (not varying with strain rate).

During the pump jet mixing of saltcake and water, waste rheology would display both Newtonian and non-Newtonian behaviors. Thus we expressed AN-105 waste viscosity as a function of strain rate and solids concentration. We did not account for thixotropic behavior because its effect on pump jet mixing was judged to be minor. Because there are six orders-of-magnitude variations in AN-105 waste viscosity, we did not find common non-Newtonian

rheology formulas (e.g., power law, Bingham model) to be able to express the ranges of measured rheology variations changing with strain rate and solid concentration. Thus we used the following expression to represent the AN-105 sludge/slurry/diluted supernatant liquid's rheology model:

$$\mu(\dot{\gamma}, C_v) = \mu_N \, exp\left(A(\beta)\left\{1 + a_1\left[1 - \frac{2}{\pi} arctan\left(a_2 \, ln\, \lambda\dot{\gamma} + a_3\right)\right]\right\}\right) \tag{2.3}$$

where

$$A(\beta) = \frac{a_4\,\beta(1+4\beta)}{1 - a_5\,\beta\left(1 - 2\beta + a_6\,\beta^2\right)}, \text{ and } \beta = \frac{C_v}{C_{vm}}$$

a_i = constants, as
a_1 = 7.6385
a_2 = 0.64215
a_3 = 4.0572
a_4 = 0.3983
a_5 = 2.8090
a_6 = 0.65936
C_v: = solid volume fraction
C_{vm} = maximum solid volume fraction = 0.2
λ: = time constant of the fluid = 0.01 s
μ: = viscosity (in Pas-sec)
μ_N = viscosity of the liquid = 0.0037 Pa-s.

Figures 2.15 and 2.16 show this AN-105 rheology model with the measured data. The AN-105 saltcake consists of 19 vol% solids (C_V=0.19). The liquid without solids corresponds to C_V= 0. In Figure 2.15, Herting's data are from Herting (1997), and Tingey's data were obtained under this current study. The ball rheometer data were taken from Stewart et al. (1996). We implemented this rheology model (Eq. 2.3) into the TEMPEST code (Onishi and Trent 1999) to simulate AN-105 pump jet mixing, as discussed in Section 4.

2.3 Solid Phase Characterization

Prior to this study, there were no direct measurements to identify solids in the AN-105 waste. Thus, we evaluated the crystallinity, morphology, chemical composition, and crystal phases of AN-105 saltcake samples with bright field image (BF), select area diffraction (SAD), and energy dispersive x-ray spectroscopy (EDS). The experimental condition was at 120 kV high tension. The magnification was up to 100KX, and the space resolution was up to 50 nm.

Examples of BF and EDS measurements of AN-105 waste are shown in Figures 2.17 and 2.18, respectively. Figure 2.17 shows the existence of $NaOH{\cdot}H_2O$ shown as "A." The EDS

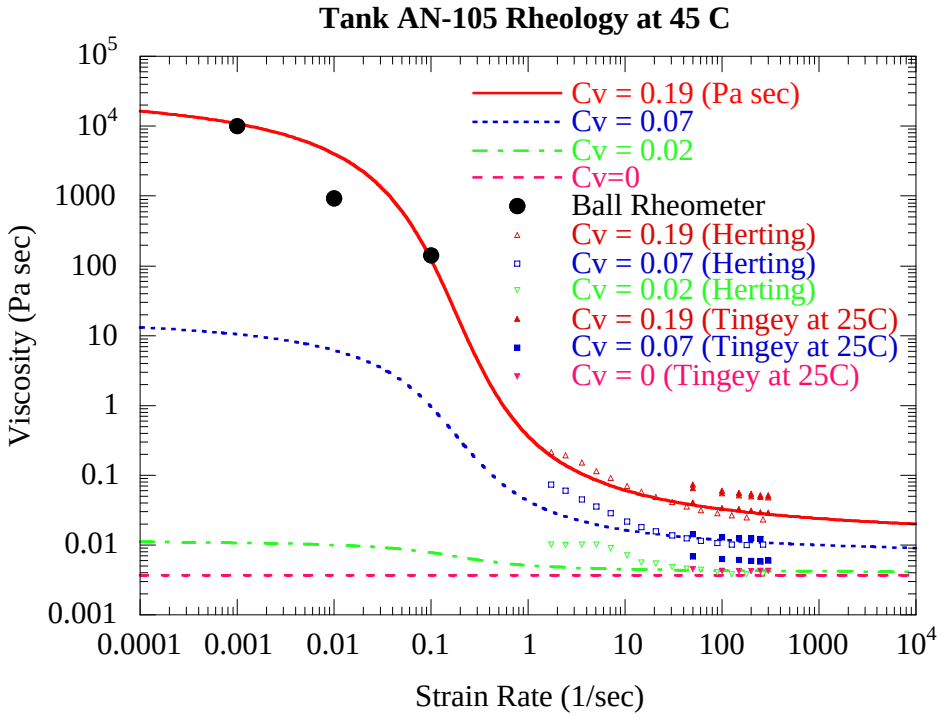

Figure 2.15. AN-105 Waste Rheology Model with Measured Viscosity Data

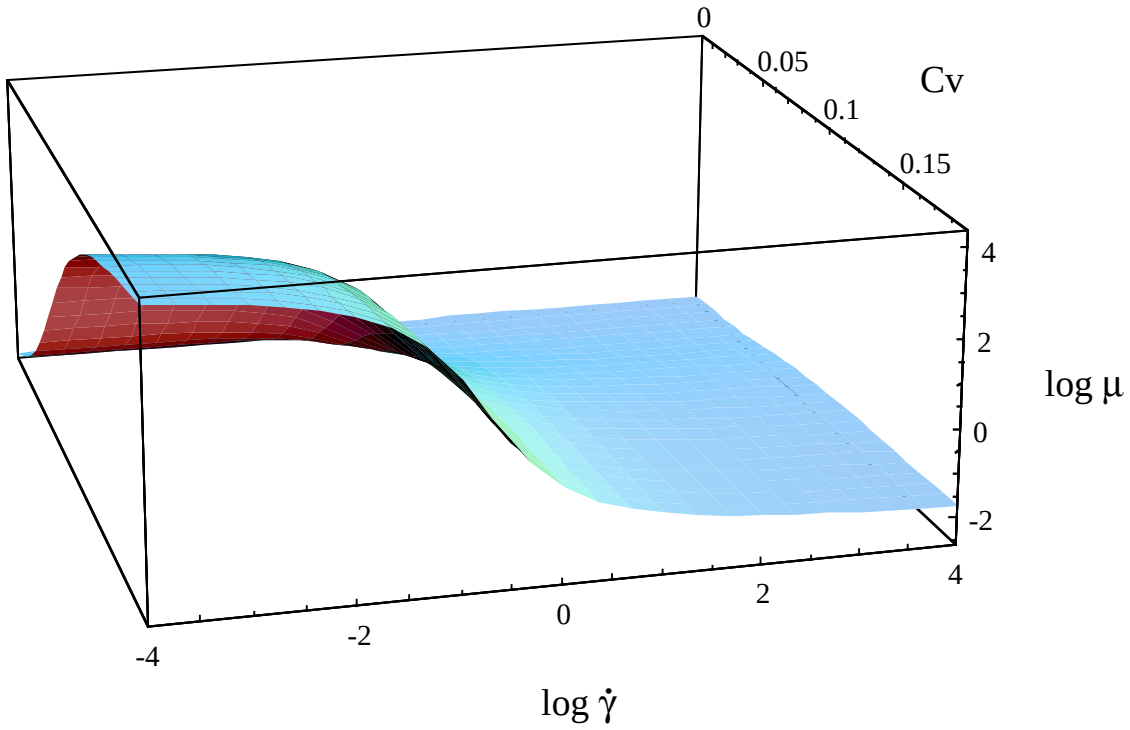

Figure 2.16. Apparent Viscosity Surface for Tank AN-105 Saltcake at 45°C

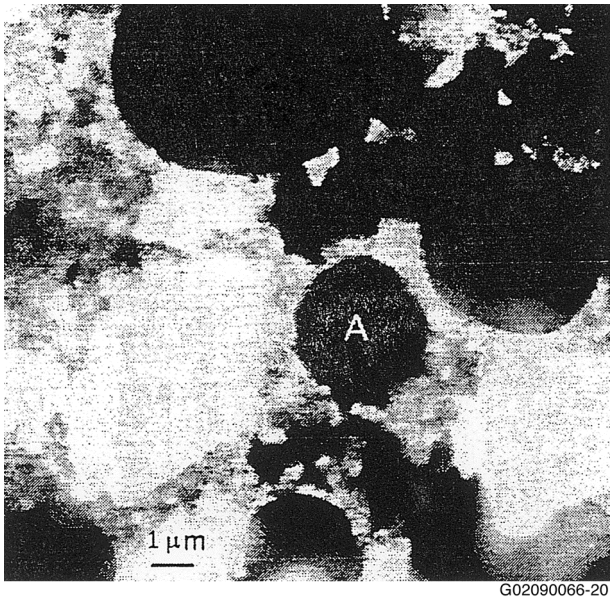

Figure 2.17. Bright Field Image Showing $NaOH \cdot H_2O$

measurement on a low magnification area of Figure 2.17 containing mixed-phase materials reveals the chemical elements Na, O, Si, Al, Mg, Cl, S, K, P, Cr, and Sr in decreasing order, as shown in Figure 2.18.

Appendix A presents AN-105 waste measurements with BF, SAD, and EDS. It is commonly believed that AN-105 saltcake contains gibbsite [$Al(OH)_3(s)$] as an aluminum solid. A surprising finding is that no gibbsite was detected, even with repeated attempts to find it in the AN-105 saltcake samples. These measurements identified magnesium silicate (possibly $Mg_8Si1_2O_{32} \cdot 4H_2O$, SiO_2), aluminum silicate, sodium aluminum silicate, calcium hydroxide, magnesium hydroxide, potassium silicate (possibly $K_2Si_2O_5$), sodium hydroxide hydrate (possibly $NaOH \cdot H_2O$), and sodium nitrate [possibly $Na_3O(NO_2)$]. However, the solid identified as sodium nitrate may be thermonatrite ($Na_2CO_3 \cdot H_2O$). Also, depending on the interpretation of the EDS measurement, there may also be thenardite (Na_2SO_4) in the AN-105 saltcake sample.

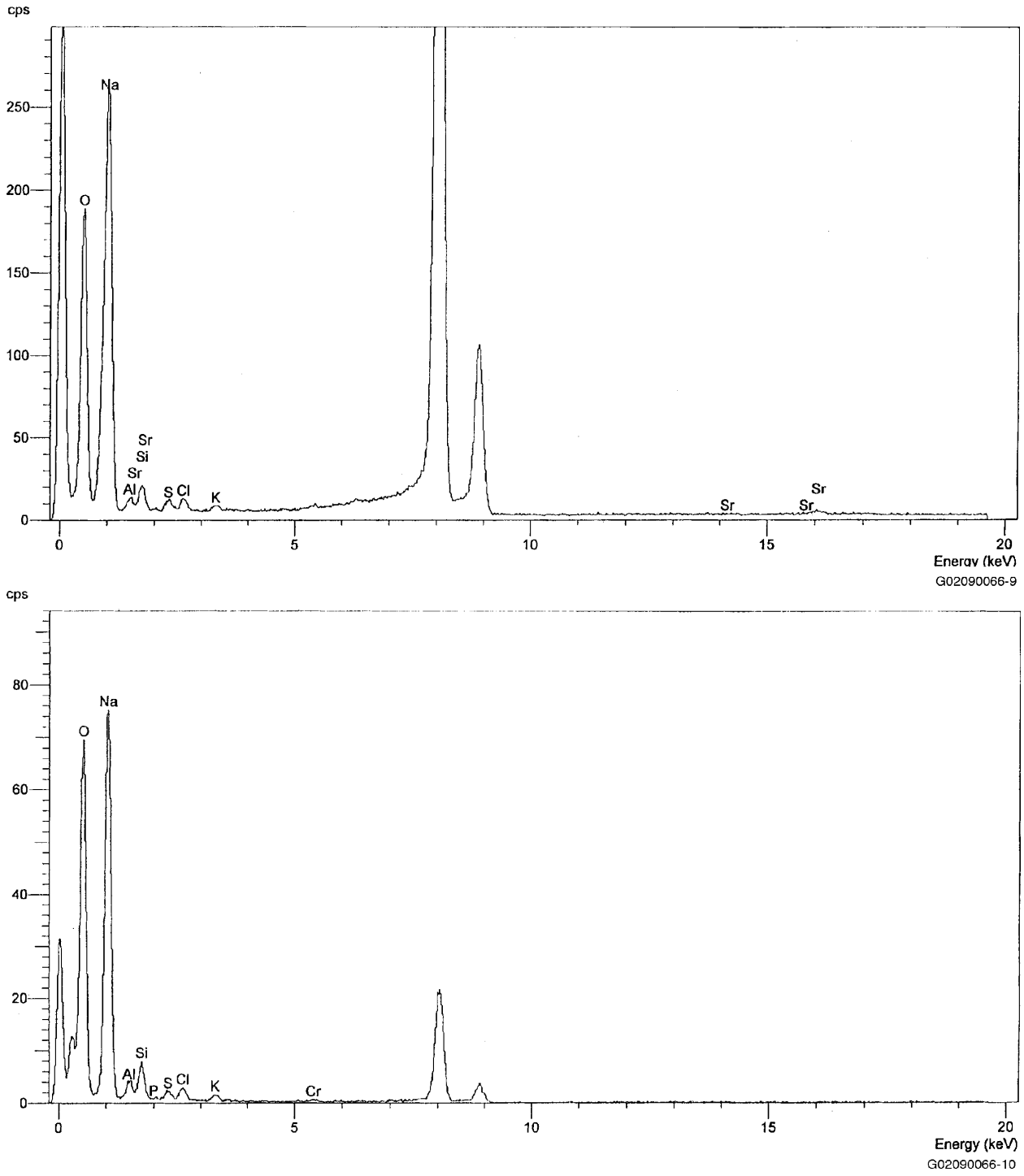

Figure 2.18. Energy Dispersive X-Ray Spectroscopy Measurement

3.0 Waste Chemistry

The AN-105 waste retrieval process involves the five steps discussed in Section 2.1. Because Steps 1, 2, and 3 affect waste chemistry, we conducted chemical modeling for the AN-105 waste by using the chemical computer code GMIN (Felmy 1995) to confirm that there would be no chemical reactions that adversely affect AN-105 pump jet mixing and pipeline transfer. The GMIN code is an equilibrium chemical model that simulates aqueous and solid chemical reactions by minimizing the Gibbs free energy and using Pitzer equations in the aqueous phase modeling. Thus, it is one of few chemical codes applicable to Hanford tank wastes having high ionic strength conditions. The following modeling steps were taken to evaluate the waste dilution with water:

- Determine solids in AN-105 saltcake layer.
- Reproduce the current chemical conditions in the supernatant liquid and solids.
- Evaluate inline dilution of AN-105 supernatant liquid with 56% water.
- Reproduce Herting's AN-105 dilution results as a validation of modeling.
- Evaluate chemical reactions of AN-105 saltcake diluted by 79 vol% water.

3.1 Current AN-105 Waste Chemistry

Before AN-105 waste chemical reactions with water were evaluated, it was required to reproduce the current AN-105 waste chemical condition with the GMIN code. Because the AN-105 supernatant liquid is expected to be in an equilibrium condition with solids in the saltcake, it was necessary first to identify solids that control the waste solution chemistry and determine the aqueous chemistry of the supernatant liquid. Tank AN-105 saltcake (solids and interstitial solution) mostly contains Al, Cl, F, Cr, K, Na, P, S, Si, inorganic carbon (expressed as a carbonate compound), and organic carbon (likely oxalate). The main ions are $Al(OH)_4^-$, Cl^-, COO^-, F^-, OH^-, NO_3^-, NO_2^-, PO_4^{3-}, and SO_4^{2-}(Jo et al. 1997; Herting 1997). Water accounts for 44.7 wt% of the saltcake. The aqueous species of the AN-105 interstitial solution within the saltcake are shown in Table 3.1, together with the aqueous chemical species and their molalities.

Based on the characterization report by Jo et al. (1997), we selected the following species for the supernatant liquid for chemical reaction modeling: $Al(OH)_4^-$, $Cr(OH)_4^-$, Na^+, CO_3^{2-}, $H_2SiO_4^{2-}$, NO_3^-, NO_2^-, SO_4^{2-}, and F^- and OH^-, $NaNO_3$(aq), and $NaNO_2$(aq). Although there is likely $Na_2C_2O_4$(s) as organic carbon, we did not simulate this solid because 1) the sodium oxalate is very insoluble so most likely its existence does not affect overall AN-105 waste chemistry, and 2) GMIN does not currently have a thermodynamic database of sodium oxalate. The measured molalities of aqueous species of the AN-105 supernatant liquid are presented in Table 3.1.

Based on the characterization report by Jo et al. (1997), dilution chemical experiments performed by Herting (1997), and our EDS, BF and SAD measurements on the AN-105 waste (see Section 2.3), we selected the following solids as potential solids in the AN-105 sludge: $Al(OH)_3$(s), $Cr(OH)_3$, $NaNO_3$(s), $NaNO_2$(s), thermonatrite [$Na_2CO_3 \cdot H_2O$(s)], thenardite (Na_2SO_4(s)), NaF(s), and amorphous SiO_2(am). Solids bearing Cd, Fe, La, Ni, U, Zr, and organic

Table 3.1. Chemical Compositions and Their Measured Concentrations for AN-105 Supernatant Liquid (estimated from Jo et al. 1997)

Compound	Measured Concentration µg/g	Selected Aqueous Species	Measured or Estimated Concentration (µg/g)	Molality
Al	23,700	$Al(OH)_4^-$	83,500	1.6934
Cr	951	$Cr(OH)_4^-$	2,200	0.0353
K	5,280	K^+	5,280	0.2602
Na	162,000	Na^+	162,000	13.5772
TIC	1,790	CO_3^{2-}	8.940	0.2871
Si	149	$H_2SiO_4^{2-}$	499	0.0102
		Cl^-	611	0.0332
		NO_2^-	73,900	3.0951
		NO_3^-	131,000	4.0708
		SO_4^{2-}	2,400	0.0481
		OH^-	40,100	4.5431

carbon (likely sodium oxalate) were treated here as insoluble solids and thus were not considered for possible dissolution or precipitation due to pump jet mixing. These solids have very low solubility limits, as evidenced by very low or below detection levels of aqueous concentrations of species bearing these solids in the interstitial solution. This assumption was judged to be reasonable and was conservative for the waste mixing and transport analyses.

We used the GMIN code to examine whether solids dissolution and precipitation would occur if only one of $Al(OH)_3$(s), $Cr(OH)_3$(am), thermonatrite [$Na_2CO_3 \cdot H_2O$(s)], $NaNO_2$(s), $NaNO_3$(s), thenardite [Na_2SO_4(s)], NaF(s), and SiO_2(am) exists in the interstitial solution. We assumed that the chemical conditions of the interstitial solution within the saltcake layer and the supernatant liquid overlaying the saltcake layer are the same, as shown in Table 3.1. If these solids did not dissolve into or precipitate from the solution, we judged these solids and the solution to be in equilibrium condition. The following are chemical simulation results for each of these potentially dissolvable solids with the solution of AN-105 saltcake.

Table 3.2 summarizes how much solids are dissolved into or precipitated from the solution to reach the solubility limit with each of the nine solids tested with the GMIN code. These model results indicate that there may be six solids in AN-105 saltcake. However, because our BF, SAD, and EDS measurements of the AN-105 saltcake did not detect gibbsite [$Al(OH)_3$(s)], we eliminated this solid. Furthermore, the amount of NaF(s) is so small that we also eliminated it from further consideration. Thus, the main solids of the AN-105 saltcake were determined to be $Na_2CO_3 \cdot H_2O$(s), Na_2SO_4(s), $Cr(OH)_3$(am), and $Ca(OH)_2$(s) in the order of abundance (in molality).

Table 3.2. Summary of Solid Testing by GMIN

Solids	Molality Dissolved	Presence among the AZ-102 Solids
Gibbsite: ($AlOH_3$(s))	0.465	Yes
$NaNO_2$(s)	5.923	No
$NaNO_3$(s)	2.497	No
NaF(s)	0.038	Yes
Themonatrite: $Na_2CO_3 \cdot H_2O$(s)	0.883	Yes
Thenardite: Na_2SO_4(s)	0.439	Yes
$Cr(OH)_3$(am)	0.034 (precipitated)	Yes
SiO_2(am)	2.24	No
$Ca(OH)_2$(s) or $CaCO_3$(s)	0.001 (precipitated)	Yes

After selecting these four solids to be solubility controlling solids, we tested potential chemical reactions with the GMIN code by putting all four together with the supernatant liquid. This is to ensure that the solids and solution used in the GMIN code reproduce the measured concentrations of aqueous chemical species and solids in AN-105. The predicted conditions of supernatant liquid and solids are presented in Figures 3.1 and 3.2 with measured data.

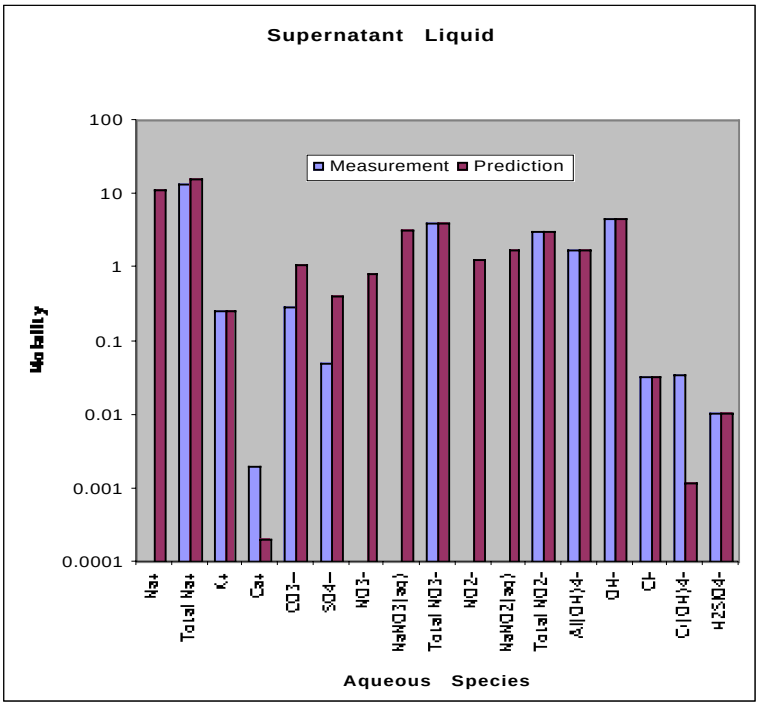

Figure 3.1. Predicted Aqueous Species Concentrations of the AN-105 Supernatant Liquid with Measured Data

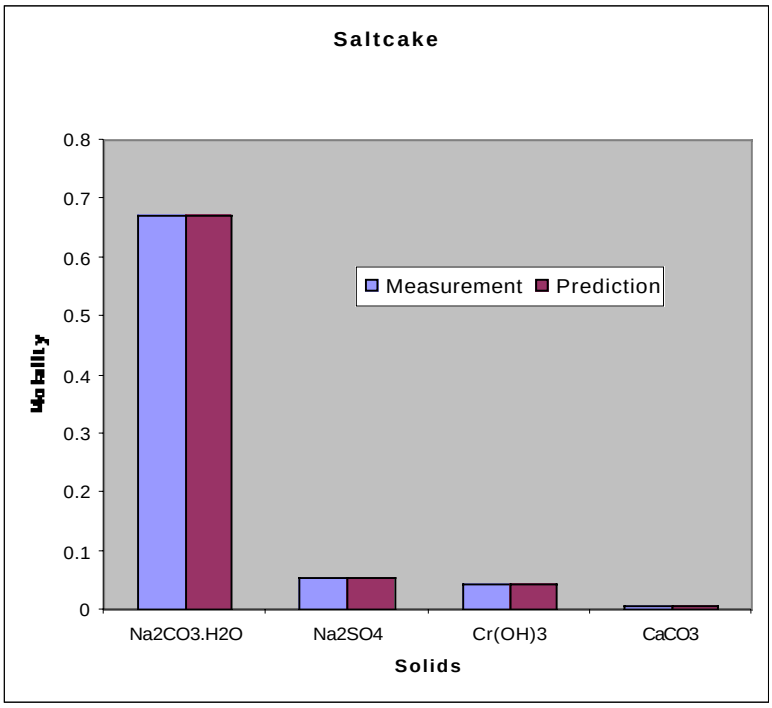

Figure 3.2. Predicted AN-105 Solid Concentrations with Measured Data

These figures show that our AN-105 waste chemistry modeling reproduced well both the supernatant liquid and saltcake. We then diluted the AN-105 supernatant liquid having these chemical characteristics by water to determine whether any chemical changes would occur.

3.2 Pipeline Inline Dilution of Supernatant Liquid with Water

The first step in waste retrieval from AN-105 would be to withdraw the supernatant liquid and dilute it with water at the beginning of the pipeline transfer. The objective of this dilution is to make the liquid waste under-saturated to avoid precipitation of solids during the pipeline transfer when the waste temperature drops. The waste dilution is expected to be at the ratio of one volume of AN-105 supernatant liquid to 0.56 volume of water. The chemical modeling with the GMIN code was performed to make sure that there would be no chemical reactions that adversely change the waste properties and hinder the pump jet mixing and pipeline transfer of the waste.

Based on this chemical modeling, the main aqueous chemical species of the supernatant liquid [Na+, CO_3^{2-}, SO_4^{2-}, OH^-, NO_3^-, $NaNO_3$(aq), NO_2^-, $NaNO_2$(aq), $Al(OH)_4^-$, Cl^-, $Cr(OH)_4^-$, $H_2SiO_4^{2-}$] are in equilibrium conditions with solids mainly consisting of $NaCO_3 \cdot H_2O$(s), $NaSO_4$(s), $Cr(OH)_3$(s), and $Ca(OH)_3$ in the AN-105 saltcake. Figure 3.3 shows the solution that results from diluting the AN-105 supernatant liquid with 56 vol% water. The model predicted that most of the aqueous chemical concentrations were reduced, including OH^- concentration. The reduction of OH^- concentration resulted in precipitation of gibbsite, which in turn made the OH^- concentration increase again slightly. However, the amount of precipitated gibbsite would

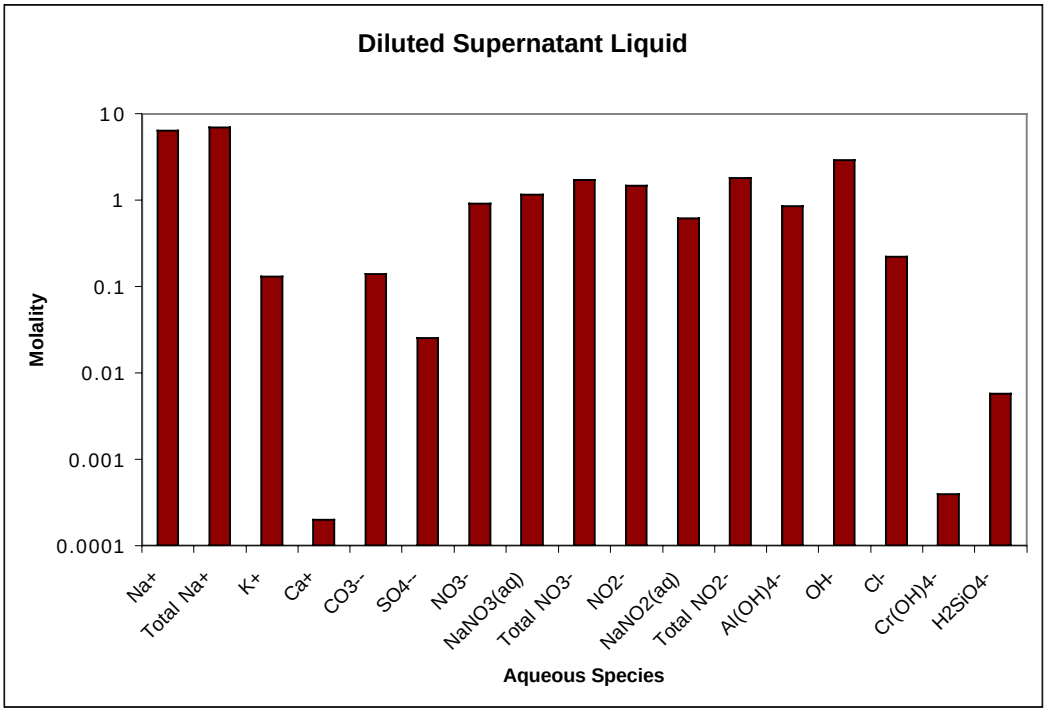

Figure 3.3. Diluted AN-105 Supernatant Liquid Resulting from 56% Inline Dilution with Water

only be about 0.3 molality. With this dilution, 0.003 molality of chromium hydroxide [$Cr(OH)_3$] was also precipitated from the diluted AN-105 supernatant liquid waste, as shown in Figure 3.4. No other solids were precipitated from this inline dilution.

As discussed in Section 2.3, the BF, EDS, and SAD measurements of AN-105 saltcake did not detect gibbsite. Herting (1997) did not report formation of gibbsite due to dilution of AN-105 WTC waste or saltcake during his dilution experiments. Thus, in spite of the chemical model's prediction of gibbsite, it is possible that gibbsite would not precipitate under this inline dilution condition. Assuming that gibbsite does precipitate, as GMIN predicts, the precipitation would produce about 75 tons of gibbsite and a very small amount of chromium hydroxide. This results in 0.6 vol% solids (density 2,420 kg/m^3) being transferred through the pipeline. We determined that mixing AN-105 supernatant liquid and water would reduce the combined liquid volume by approximately 0.3%, based on AN-104 experiments conducted by Herting (1998).

With 0.6 vol% gibbsite in the diluted AN-105 waste having an expected viscosity of 10 cP, we estimated the critical velocity would be approximately 0.3 m/s (1 ft/sec) to maintain turbulence flow, as recommended by Wasp et al. (1977). Thus there would be no solids deposition in the pipeline when the expected velocity is about 1.2–1.8 m/s (4–5 ft/sec) (Julyk et al. 2002). Although at the early stage of gibbsite formation solids may be sticky, gibbsite precipitation may be too slow (likely days to weeks) to be a concern during the waste pipeline transfer.

These evaluations indicate that there would be no adverse impact on the AN-105 supernatant liquid properties that hinder waste pipeline transfer due to inline dilution with water.

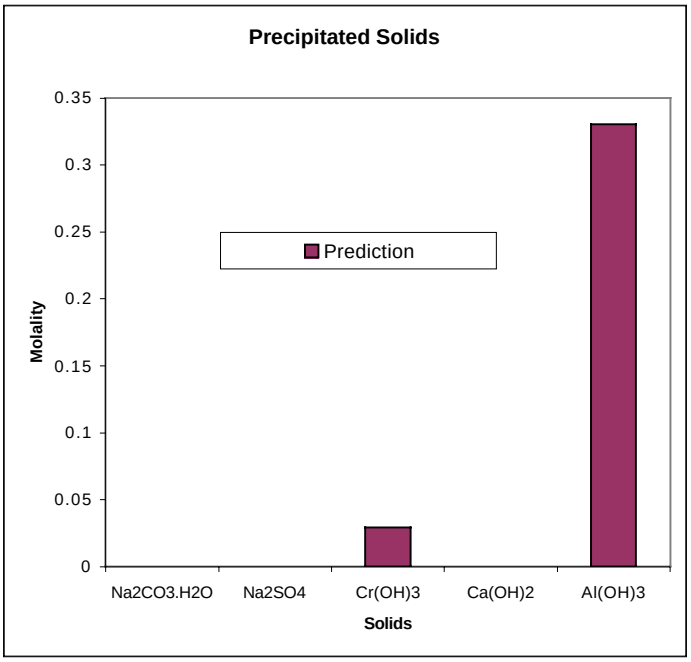

Figure 3.4. Solids Precipitated from AN-105 Supernatant Liquid by 56-vol% Inline Dilution with Water

3.3 In-Tank Dilution of AN-105 Saltcake with Water

After retrieving the AN-105 supernatant liquid with inline dilution, the remaining waste (saltcake) would be diluted with water within the tank, as described in Section 2.1. The mixing ratio for in-tank dilution is expected to be 1 volume of saltcake to 0.79 volume of water (Orme et al. 2001). Prior to evaluating the AN-105 saltcake in-tank dilution, we first tested GMIN with experimental data.

3.3.1 Chemical Model Testing with Dilution Experiments

Prior to applying the GMIN chemical code to the AN-105 conditions, we compared chemical modeling with AN-105 dilution experimental data (Herting 1997). The experiments include dilution of the both WTC samples and saltcake samples.

Figure 3.5 shows the amounts of solids (in molality) in 1) the original WTC, 2) 50% diluted WTC without chemical reactions, and 3) 50% diluted WTC with chemical reactions (1 volume of WTC and 0.5 volume of water). The main solids in the AN-105 waste are $Na_2CO_3 \cdot H_2O$(s) and Na_2SO_4(s), which were predicted to be totally dissolved. $Cr(OH)_3$(am) and $Ca(OH)_2$(s) did not precipitate or dissolve with the added water.

Figure 3.6 shows the amounts of solids (in molality) in 1) the original saltcake, 2) 80%-diluted saltcake without chemical reactions, and 80%-diluted saltcake with chemical reactions when AN-105 saltcake is diluted by 80% of water (1 volume of saltcake and 0.8 volume of

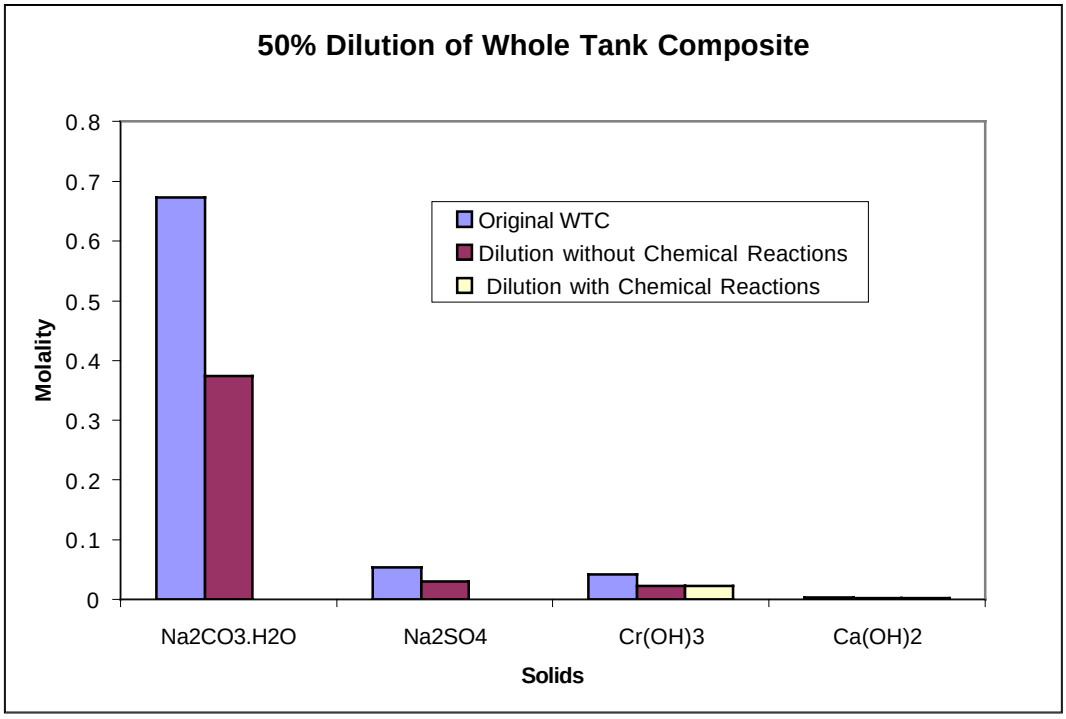

Figure 3.5. Solid Amount Changes Due to 50% Dilution of AN-105 Whole Tank Composite Waste with Water

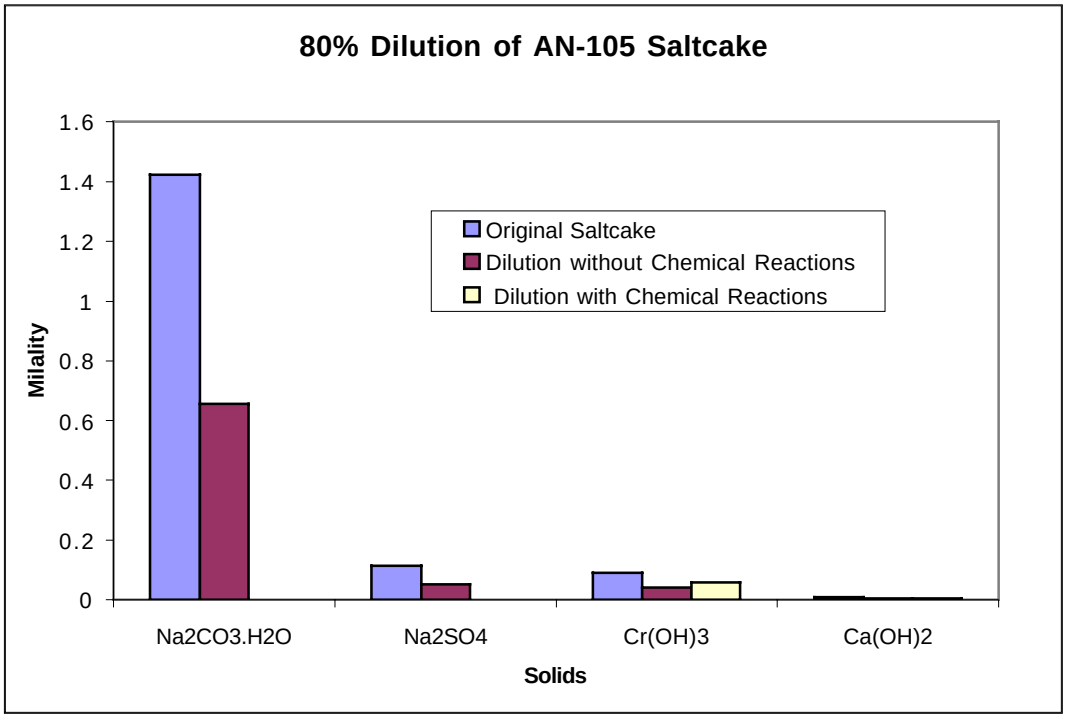

Figure 3.6. Solid Amount Changes due to 80% Dilution of AN-105 Saltcake with Water

water). Like the 50% WTC dilution by water, $Na_2CO_3 \cdot H_2O(s)$ and $Na_2SO_4(s)$ are predicted to be totally dissolved, as shown in Figure 3.5. $Cr(OH)_3(am)$ was predicted to be very slightly precipitated (0.016 m), while $Ca(OH)_2(s)$ neither precipitate nor dissolved due to the added water. The chemical modeling also predicted that 40% dilution of the AN-105 saltcake with water would also dissolve all the $Na_2CO_3 \cdot H_2O(s)$ and $Na_2SO_4(s)$, as shown in Figure 3.6.

The predicted solid dissolution and precipitation matched reasonably well with measured data, as shown in Table 3.3. We then assessed AN-105 saltcake dilution with the waste characteristics reported in the *AN-105 Tank Characterization Report* (Jo et al. 1997), which presents somewhat different waste chemistry than reported by Herting (1997).

Table 3.3. Comparison of Measured and Predicted Changes on Solid Amounts Due to 50% Dilution of AN-105 Waste WTC with Water

		Solids (molality)			
		$Na_2CO_3 \cdot H_2O$	Na_2SO_4	$Cr(OH)_3$	$Ca(OH)_2$
WTC 50% Dilution	Experiments	All dissolved	All dissolved	No change	No change
	Prediction	All dissolved	All dissolved	No change	No change
Saltcake 80% Dilution	Experiments	All dissolved	All dissolved	No change	No change
	Prediction	All dissolved	All dissolved	Very slightly precipitated (0.016 m)	No change

3.3.2 79% In-Tank Dilution

After the supernatant liquid has been removed from Tank AN-105 with inline dilution, the remaining saltcake waste is expected to be diluted by 79% water in the tank (see Steps 2 and 3 described in Section 2.1). We predicted the potential chemical changes to make sure that the in-tank dilution would dissolve a large amount of solids and that these chemical changes would not adversely affect the subsequent waste retrieval and pipeline transfer.

With the chemistry reported in the Tank AN-105 Characterization Report (Jo et al. 19997) as a starting condition, we simulated chemical reactions due to saltcake dilution with water. Figures 3.7 and 3.8 show the model predictions. Similar to the results discussed in Section 3.3.1, all $Na_2CO_3 \cdot H_2O(s)$ and $Na_2SO_4(s)$ are dissolved. Only small amounts of $Cr(OH)_3(am)$ and $Ca(OH)_2(s)$ and possibly sodium oxalate [$Na_2C_2O_4(s)$] remain as main solids in the saltcake.

These remaining solids [$Cr(OH)_3(am)$, $Ca(OH)_2(s)$, and possibly $Na_2C_2O_4(s)$] would settle without forming a gel (Step 4 of the waste retrieval) and would be separated from the supernatant liquid. Thus, it is feasible to retrieve the resulting supernatant liquid from 79% in-tank dilution of the saltcake from AN-105 and to transfer it through a 3-inch (0.07-m) pipeline.

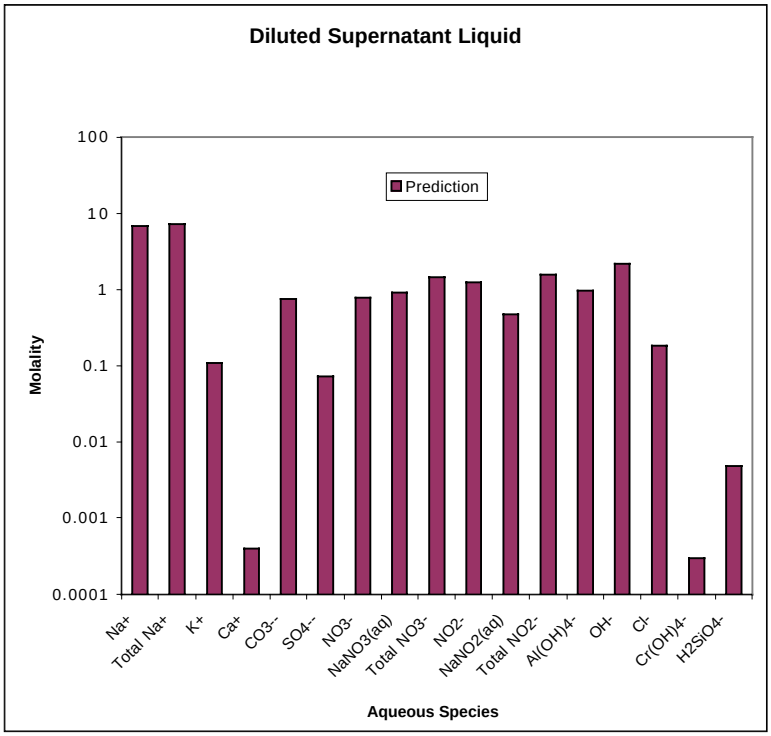

Figure 3.7. Resulting Supernatant Liquid Chemistry after 79% Dilution of AN-105 Saltcake by Water

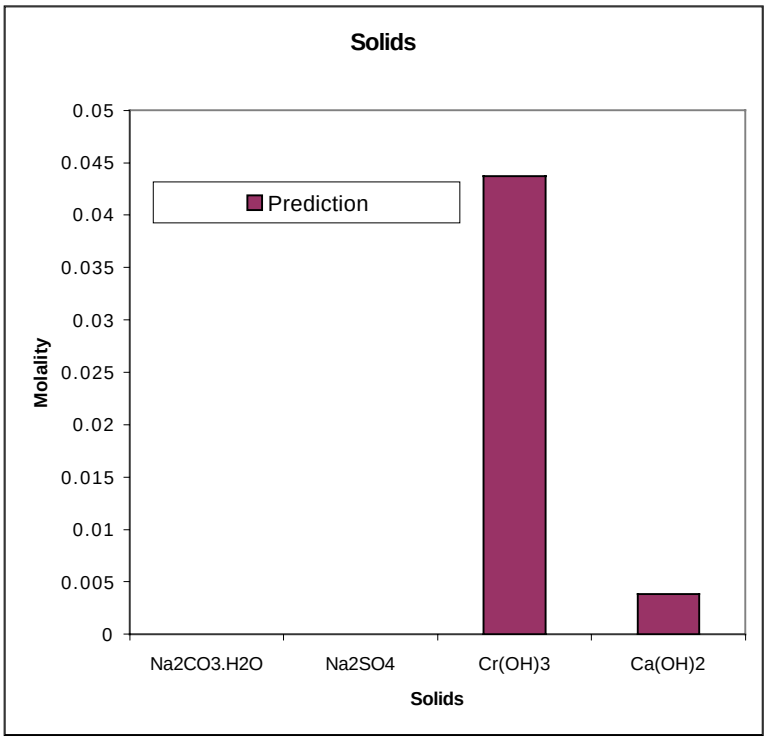

Figure 3.8. Resulting Saltcake after 79% Dilution of AN-105 Saltcake by Water

4.0 Waste Pump Jet Mixing Evaluation

We evaluated how much AN-105 waste would be mix by two off-centered, 300-hp mixer pumps when the AN-105 saltcake is mixed with water at the ratio of 1 volume of saltcake to 0.79 volume of water. We used the time-varying, three-dimensional TEMPEST code (Onishi and Trent 1999) to simulate mixing of saltcake and water by the pumps. The viscosity formula (Eq. 2.3) was implemented to TEMPEST. Because two mixer pumps are 20 ft (6.1 m) away from the tank center on opposite sides of the tank and rotate at 0.2 rpm in a synchronized mode, we simulated the right half of the tank based on symmetry.

Chemical modeling results presented in Section 3 indicate that over 90% of the solids [all thermonatrite ($Na_2CO_3 \cdot H_2O$) and thenardite (Na_2SO_4)] would be dissolved. This significant reduction of solid volume and expected reduction of the yield strength of saltcake would make it easier for mixer pumps to mobilize the AN-105 saltcake. Nonetheless, we assigned the waste properties and saltcake volume to be the same as the current values discussed in Section 2 as a conservative evaluation. This includes using the AN-105 specific viscosity formula (Eq. 2.3) in the modeling. We assigned the yield strength to be 100 Pa (a conservative value considering the solid dissolution occurring during mixing). Furthermore, this model used baseline mixer pumps that had the injection nozzles at the top and the inlet at the bottom, as shown in Figure 2.2, instead of the redesigned "inverted" mixer pumps with the injection nozzles at the bottom and inlet at the top because the simulation was performed before the Hanford Site adapted this new pump configuration. However, as reported in Onishi et al. (2002), the redesigned mixer pumps are somewhat more effective than the former baseline pumps at eroding solids. Thus the simulation results with the baseline pump configuration are also somewhat conservative.

As noted in Section 2.1, the AN-105 model divides AN-105 solid particles into four sizes (see Table 2.1). Because the total solid volume fraction (sum of solids 1 through 4) in the saltcake was assigned to be 19 vol% and solid 4 makes up 25% of the total solids, solid 4 occupies 4.81 vol% in the saltcake. Similarly solids 1 through 3 occupy 5.21, 6.51, and 2.47 vol%, respectively, in the saltcake. Because solid 4 is the largest, it is the most difficult to suspend uniformly in the tank. We present simulation results with solid 4 in this section.

The upper plot of Figure 4.1 shows the initial distributions of velocity and volume concentrations of solid 4 on a vertical plane (vertical plane 2) containing the pump center and the tank wall nearest to the 20-ft (6.1-m), off-center pump. We assigned this position to be in 3 o'clock position and 0°, from which other vertical planes were measured. The lower plot Figure 4.1 shows the initial conditions on vertical plane 14. The mixer jets must travel the longest distance (44 ft or 13 m) to reach the tank wall along vertical plane 14 (108° from vertical Plane 2).

This figure shows the initial 177- inch (4.5-m) thick saltcake layer at the tank bottom and 140-inch (3.55-m) thick water layer, totaling 317 inches (8.05-m) in Tank AN-105. It also shows the positions of one of the two rotating pumps, its withdrawal inlet located seven inches (0.18 m) above the tank bottom, and a six-inch (0.15-m) nozzle (located 18 inches or 0.46 m above the tank bottom) injecting a 60-ft/sec (18.3-m/s) jet into the saltcake layer.

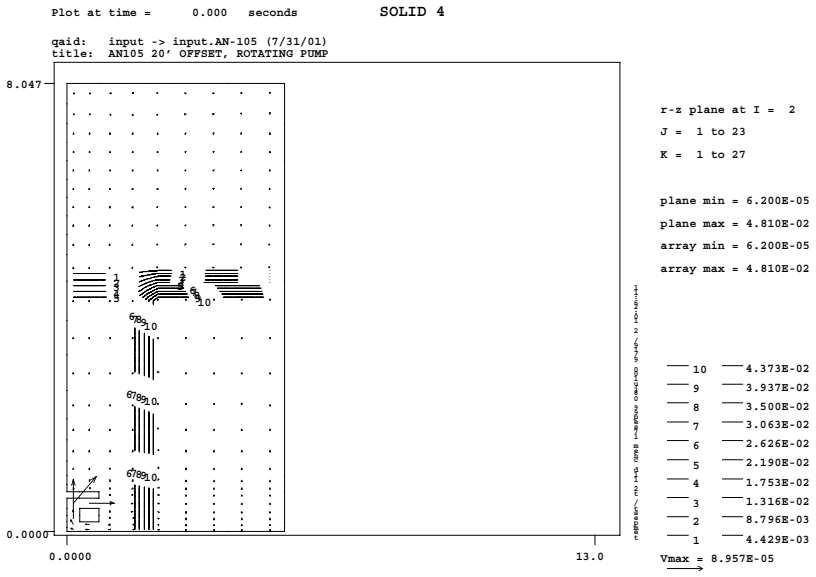

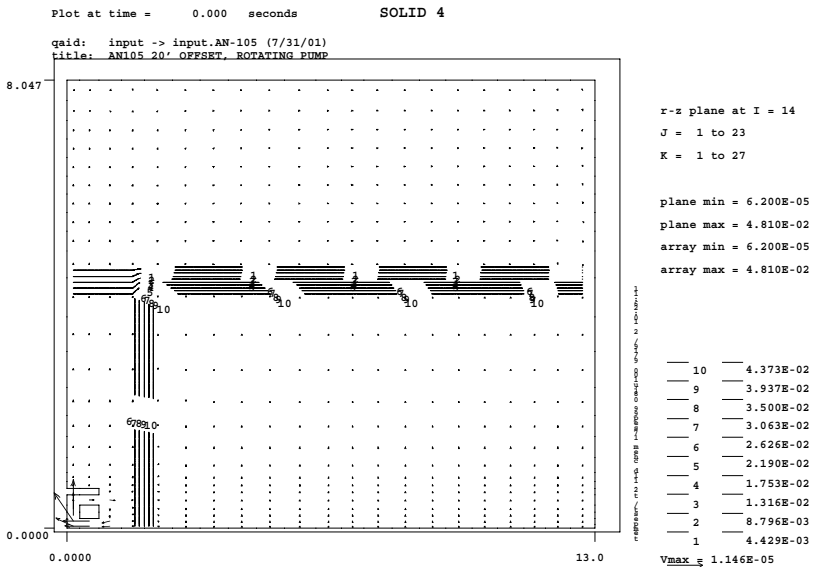

Figure 4.1. Initial Conditions of Saltcake and Water on Vertical Plane 2 (upper plot oriented at 3 o'clock position) and Vertical Plane 14 (lower plot oriented at 108° counterclockwise from vertical plane 2)

The tank boundary is also indicated in this figure by the solid line, and the presence of the velocity vector indicates that its location is within the tank. The solid 4 concentration within the saltcake layer is 4.81 vol%, as shown in this figure. The initial solid concentration in the liquid layer was assigned a small value (0.0062 vol%) rather than zero for the TEMPEST code to accommodate the settling velocity of the solids for all solid concentrations.

The tops of both plots of Figure 4.1 show the time (0 simulation second in these plots) and the solid concentration as volume fraction (volume fraction of one being 100 vol%). The left side of the figure describes which vertical plane it is showing (in the upper plot it is a r-z plane, or vertical plane 2 (I=2), oriented at the 3 o'clock position, and in the lower plot it is r-z plane, or vertical plane 14 (I=14), 108° counterclockwise from vertical plane 2), and an area of the plot coverage on these vertical planes (in this case J=1 to 23, indicating the entire horizontal direction from the pump center to 13 m way, and K=1 to 27, indicating the vertical direction from the tank bottom to the waste surface at 8.047 m). The right side of these plots also shows solid concentrations (expressed in volume fractions) represented by Lines 1 through 10. Plane min and max indicate the minimum and maximum values (solid volume fractions of 6.2×10^{-5} (or 0.0062 vol%) and 0.0481 (or 4.81 vol%), respectively, in this case) within the plotted planes, while array min and max indicate the minimum and maximum values (solid volume fractions of $6.2X10^{-5}$ (or 0.0062 vol%) and 0.0481 (or 4.81 vol%), respectively, in this case) encountered within the entire tank simulation area. As shown in these two plots, we diluted the saltcake in the immediate vicinity of the mixer pumps as the initial condition to reflect waste conditions after the mixer pumps had been installed in the tank but before they starting mixing the waste.

At the right bottom of these two plots, the maximum velocities appeared on these vertical planes are shown (in this case 8.957×10^{-5} and 1.146×10^{-5} m/s with its corresponding scale lengths). All velocity magnitude in these plots is scaled to this magnitude. Note that the jet velocity at the nozzle exit was assigned to be 60 ft/sec (18.3 m/s) during the simulation.

Predicted vertical distributions of velocities and solid 4 concentrations on vertical planes 2 and 14 at 3.4 simulation minutes are shown in Figure 4.2. At this time, the rotating mixer jets hit vertical plane 2 (top plot) once and are hitting vertical plane 14 a second time, mobilizing some saltcake. (The rotating jet is oriented along vertical plane 14 (bottom plot) at this time with a maximum velocity of 15.4 m/s. The velocity indicated on this plot is cell-centered, thus showing a somewhat smaller value than the 18.3-m/s velocity the model was actually using.) On vertical plane 2, the mixer jet already mobilized some of the saltcake along the tank wall because this plane has the shortest distance (17.5 ft or 5.3 m) to the tank wall. On the other hand, the mixer jet has not mobilized most of the saltcake on the right side of the tank because the jet must travel the longest distance (44 ft or 13 m) to reach the tank wall on this plane.

Predicted vertical distributions of velocities and solid 4 concentrations on vertical planes 2 and 14 at 10 simulation minutes are shown in Figure 4.3. At 10 simulation minutes, one of the rotating mixer jets is again hitting vertical plane 2, but the solid concentration still has large vertical gradient. On vertical plane 14, the mixer jet has just reached the tank wall to start mobilizing the solids at the farthest corner of the tank.

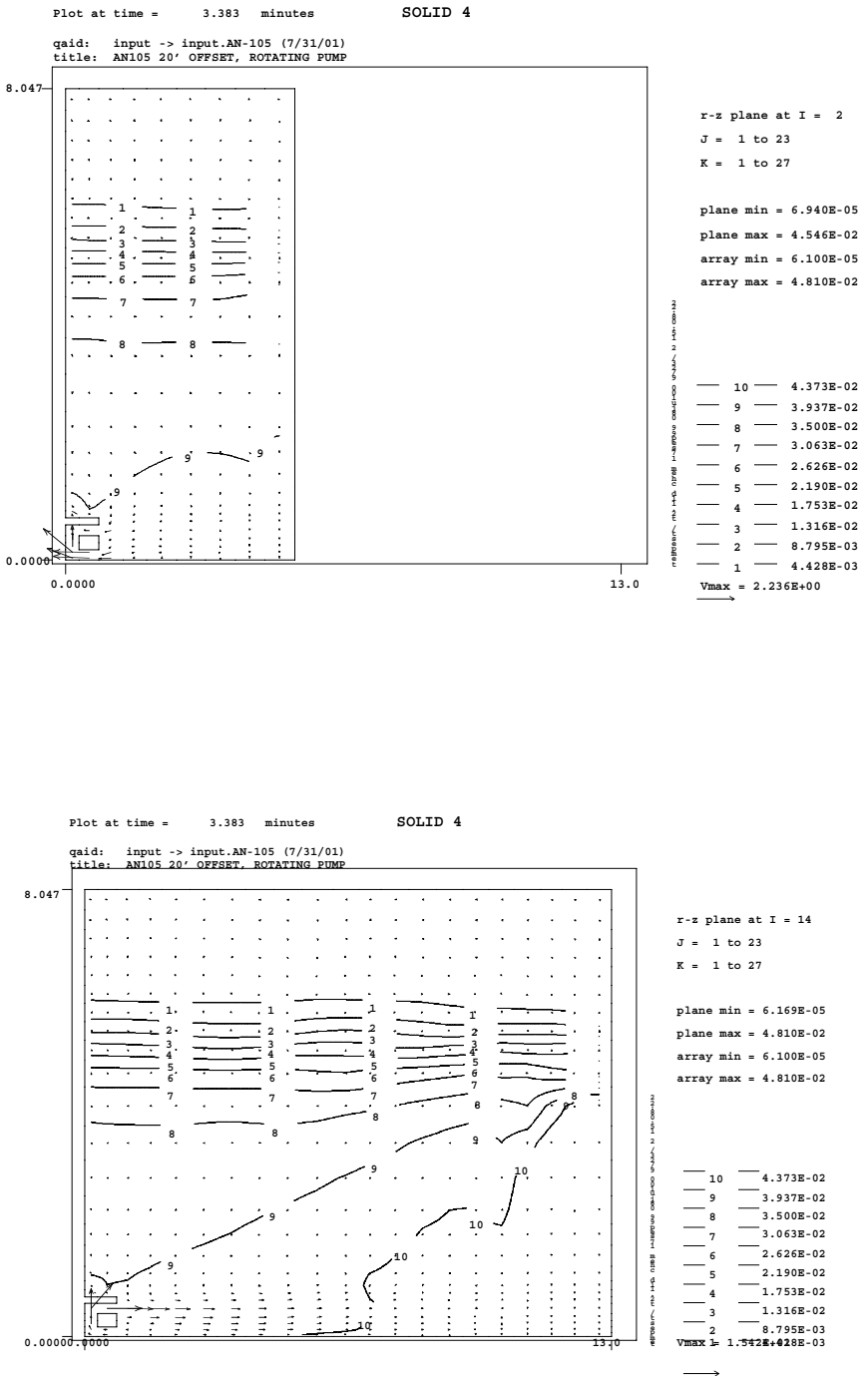

Figure 4.2. Predicted Distributions of Velocity and Solid 4 Concentration on Vertical Plane 2 (upper plot oriented at 3 o'clock position) and Vertical Plane 14 (lower plot oriented at 108° counterclockwise from vertical plane 2) at Three Simulation Minutes

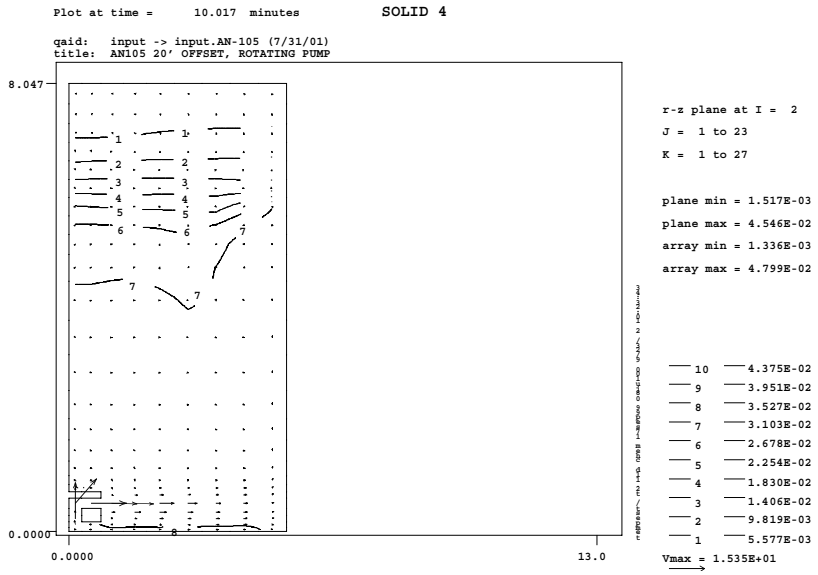

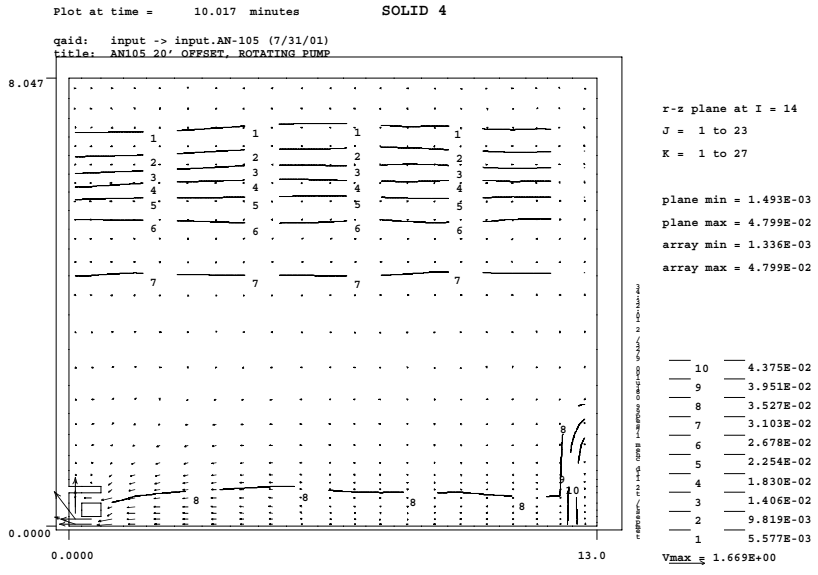

Figure 4.3. Predicted Distributions of Velocity and Solid 4 Concentration on Vertical Plane 2 (upper plot oriented at 3 o'clock position) and Vertical Plane 14 (lower plot oriented at 108 ° counterclockwise from vertical plane 2) at 10 Simulation Minutes

At 30 simulation minutes, mixer jets mobilized all the solids, and the solids are fully mixed over the entire tank. (At this time, the rotating jet is oriented along vertical plane 2.) This is clearly shown in Figure 4.4, depicting the velocity and Solid 4 concentrations on vertical planes 2 and 14. At this time, solid 4 has the uniform concentration of 2.6 vol%. Note that on vertical plane 2 (the upper plot of Figure 4.4), the plane maximum concentration is listed as 4.546 vol%, instead of 2.6 vol%. This is because a speck of solids was accumulated on the upper corner of the pump. Except this very small spot, the solid concentration is uniform (2.6 vol%) throughout the entire tank.

Figures 4.5 through 4.7 show predicted velocity and concentrations of solids 1 through 3, respectively, at 30 simulation minutes. These figures also show that all solids are uniformly distributed within the tank, except again at the upper corner of the pump on plane 2. The uniform concentrations of solids 1 through 3 are 3.2, 2.6, and 2.0 vol%, respectively. Thus, the total solid concentration (sum of solids 1 through 4) is 10.4 vol%.

These AN-105 pump jet mixing model results indicate that two 300-hp mixer pumps would erode all AN-105 saltcake and uniformly distribute it over the entire tank even under the conservative conditions imposed in this evaluation.

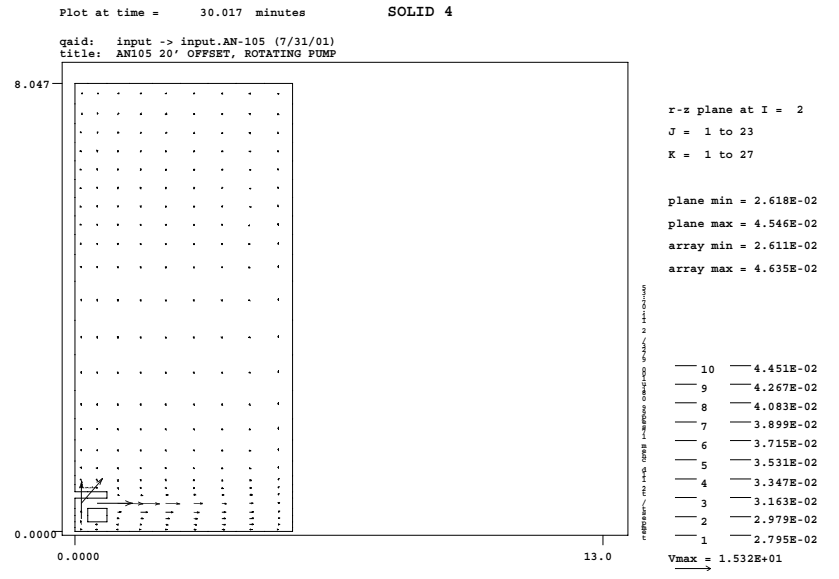

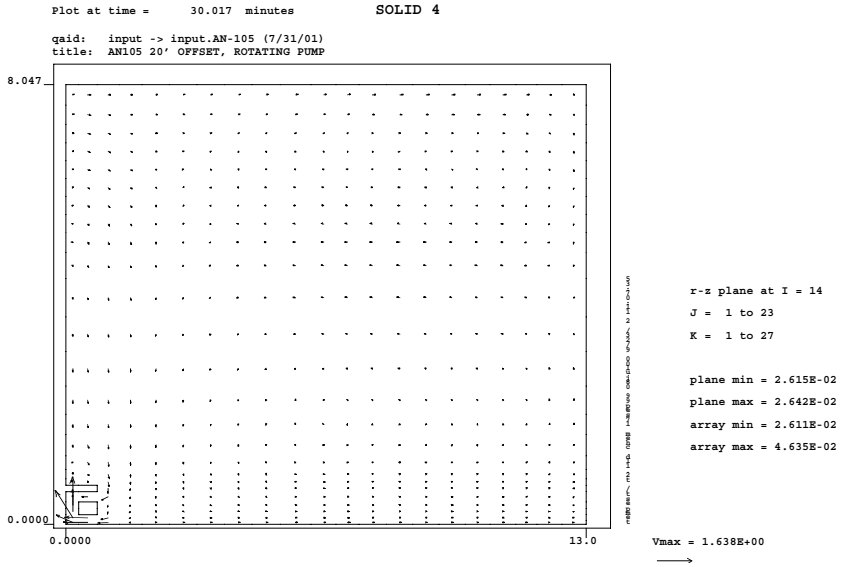

Figure 4.4. Predicted Distributions of Velocity and Solid 4 Concentration on Vertical Plane 2 (upper plot oriented at 3 o'clock position) and Vertical Plane 14 (lower plot oriented at 108 ° counterclockwise from vertical plane 2) at 30 Simulation Minutes

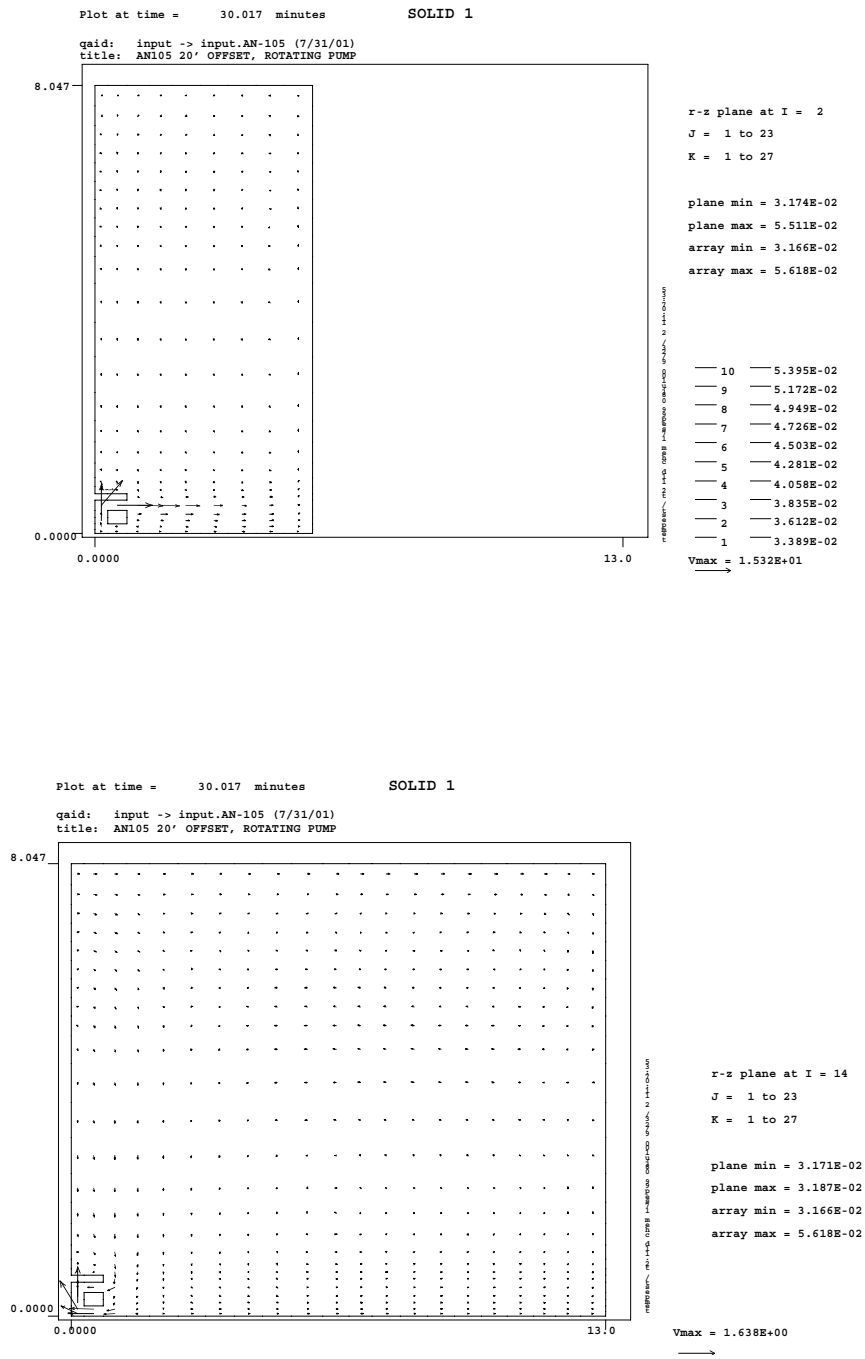

Figure 4.5. Predicted Distributions of Velocity and Solid 1 Concentration on Vertical Plane 2 (upper plot oriented at 3 o'clock position) and Vertical Plane 14 (lower plot oriented at 108° counterclockwise from vertical plane 2) at 30 Simulation Minutes

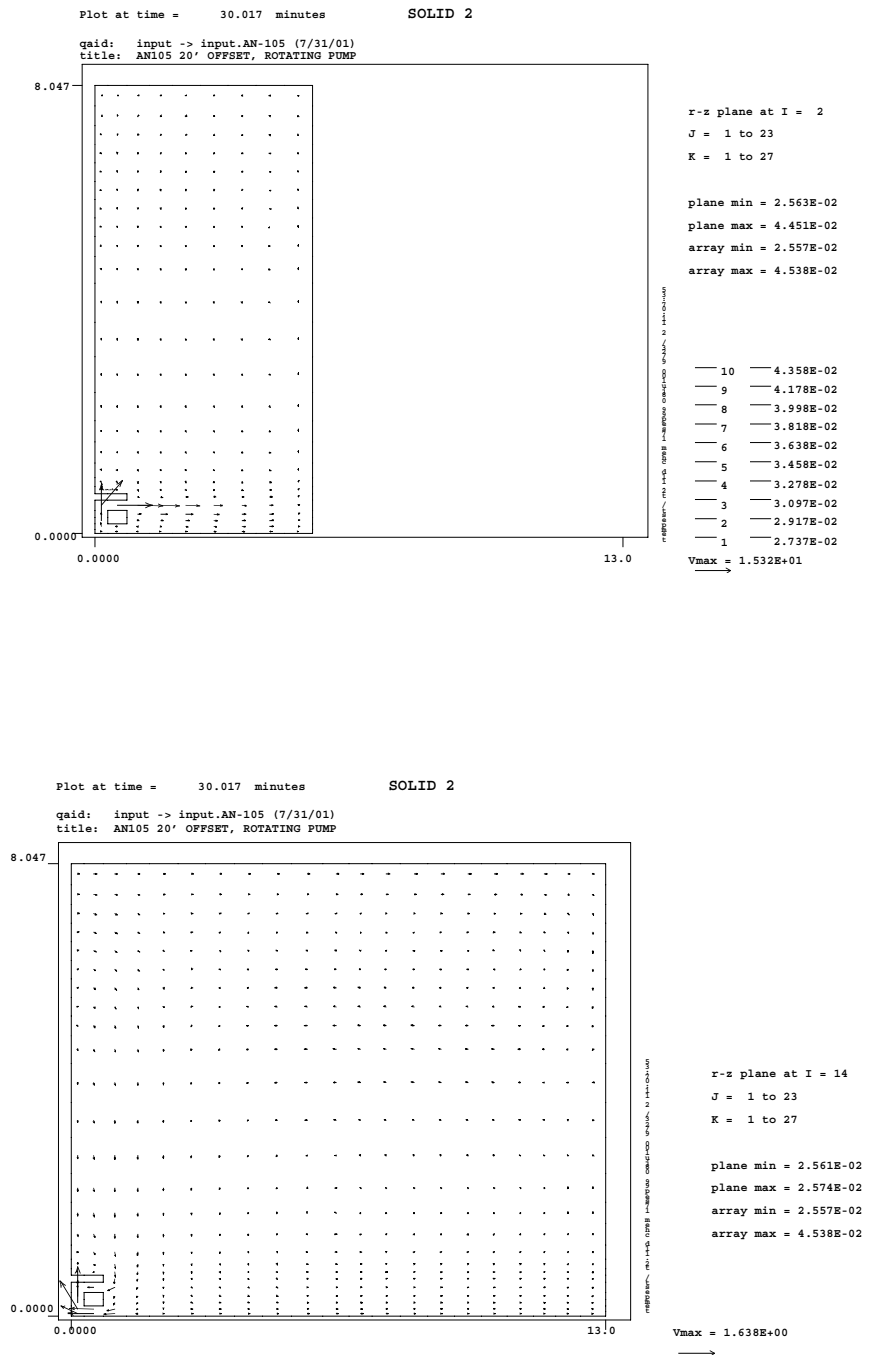

Figure 4.6. Predicted Distributions of Velocity and Solid 2 Concentration on Vertical Plane 2 (upper plot oriented at 3 o'clock position) and Vertical Plane 14 (lower plot oriented at 108° counterclockwise from vertical plane 2) at 30 Simulation Minutes

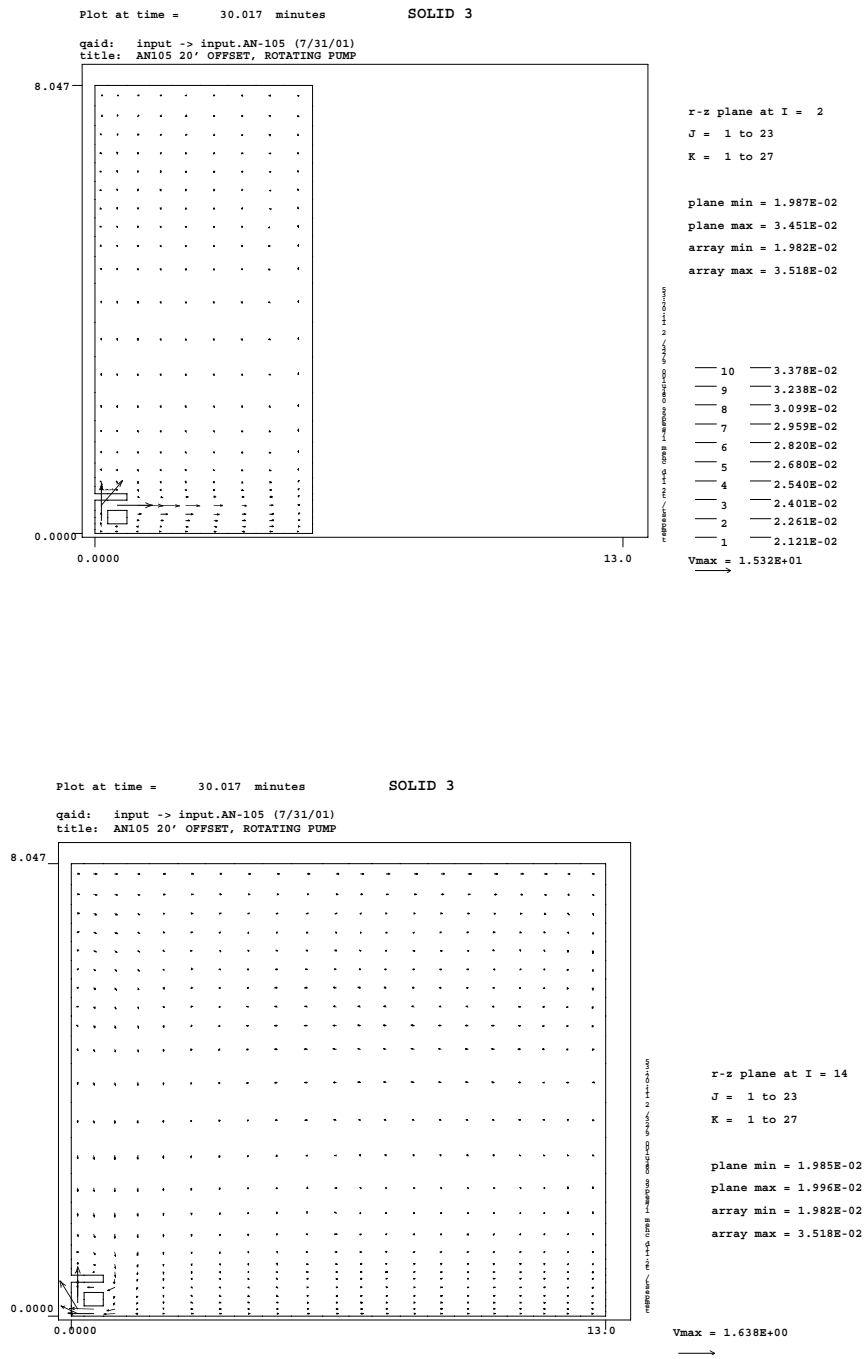

Figure 4.7. Predicted Distributions of Velocity and Solid 3 Concentration on Vertical Plane 2 (upper plot oriented at 3 o'clock position) and Vertical Plane 14 (lower plot oriented at 108° counterclockwise from vertical plane 2) at 30 Simulation Minutes

5.0 Slurry Waste Pipeline Transfer

The current retrieval plan for AN-105 waste is to remove 1) the inline-diluted supernatant liquid and 2) the supernatant liquid resulting from in-tank dilution of the saltcake. As discussed in Sections 3.2 and 3.3, these waste transfers are feasible with no adverse problems. In addition to these liquid pipeline transfer cases, we also evaluated a scenario in which AN-105 solid-liquid slurry waste was transferred to Tanks AP-102 and AP-104.

5.1 Four Scenarios

In case the mixed AN-105 waste was transferred, we also evaluated transferring the AN-105 waste slurry through a 3-inch pipeline to the AP Tank Farm. We selected the following slurry conditions:

- Fully mixed AN-105 waste (bulk density of 1.5 g/mL)
- Fully mixed AN-105 waste diluted by 25 vol% water (bulk density of 1.4 g/mL)
- Fully mixed AN-105 waste diluted by 50 vol% water (bulk density of 1.35 g/mL)
- Fully mixed AN-105 waste diluted by 100 vol% water (bulk density of 1.25 g/mL).

Because kinetic reaction testing was performed with small quantities (Herting 1997), it is not certain that chemical dissolution/precipitation reactions would be completed at the beginning of the diluted AN-105 slurry pipeline transfer. Thus, we considered the following seven cases:

- Case 1. AN-105 fully mixed waste without any dilution
- Case 2. AN-105 fully mixed waste with 25% dilution with solids dissolution
- Case 3. AN-105 fully mixed waste with 25% dilution without solids dissolution
- Case 4. AN-105 fully mixed waste with 50% dilution with solids dissolution
- Case 5. AN-105 fully mixed waste with 50% dilution without solids dissolution
- Case 6. AN-105 fully mixed waste with 100% dilution with solids dissolution
- Case 7. AN-105 fully mixed waste with 100% dilution without solids dissolution.

5.2 Waste Properties

We used the AN-105 waste rheology (changing with solids concentration and strain rate) expressed as Equation (2.3) discussed in Section 2.2.3. Figure 5.1 shows the viscosity variation, including the viscosity of the fully mixed AN-105 waste, as shown by the solid line. There is no yield strength in the fully mixed or diluted AN-105 composite waste, as discussed in Section 2.2.2 (see Figure 2.10). The waste property values used for the slurry transfer evaluation are shown in Table 5.1.

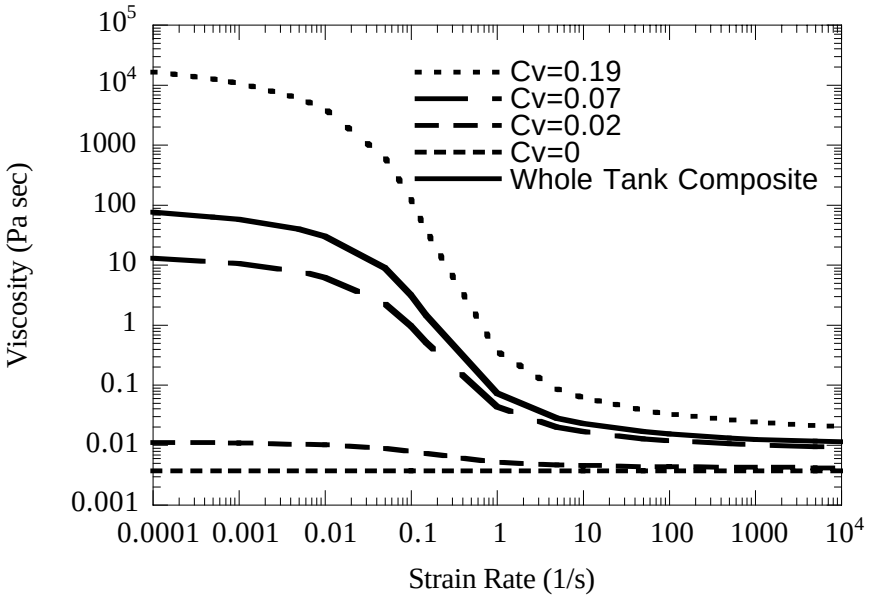

Figure 5.1. AN-105 Waste Rheology

Table 5.1. An-105 Slurry Transfer Waste Property Values

Waste Property	Case 1	Case 2	Case 3	Case 4	Case 5	Case 6	Case 7
Dilution water	0	25	25	50	50	100	100
Solids dissolution	No	No	Yes	No	Yes	No	Yes
Liquid density, kg/m^3	1,430	1,338	1,370	1,278	1,320	1,206	1.290
Liquid viscosity, cP	3.7	3.1	3.3	2.7	3.0	2.3	2.8
Solids density, kg/m^3	2,300	2,300	2,300	2,300	2,300	2,300	2,300
Solids volume, %	8.21	6.57	4.43	5.47	3.28	4.11	2.79
Solid size distribution, μm	Vol%						
0.5	4.98	4.98	11.40	4.98	5.73	4.98	5.73
1.5	15.97	15.97	20.90	15.97	13.90	15.97	13.90
2.5	9.64	9.64	14.00	9.64	11.00	9.64	11.00
3.5	11.97	11.97	15.60	11.97	12.70	11.97	12.70
4.5	8.88	8.88	15.20	8.88	12.20	8.88	12.20
5.5	5.97	5.97	7.82	5.97	6.33	5.97	6.33
6.5	5.69	5.69	5.39	5.69	3.29	5.69	3.29
7.5	2.72	2.72	2.80	2.72	1.21	2.72	1.21
8.5	1.39	1.39	1.62	1.39	1.32	1.39	1.32
9.5	1.95	1.95	0.87	1.95	0.62	1.95	0.62
15.0	8.72	8.72	3.70	8.72	6.39	8.72	6.39
25.0	5.60	5.60	0.25	5.60	7.66	5.60	7.66
35.0	0	0	0	0	8.36	0	8.36
45.0	7.21	7.21	0	7.21	9.29	7.21	9.29
55.0	4.55	4.55	0	4.55	0	4.55	0
65.0	4.76	4.76	0	4.76	0	4.76	0
Mixture density, kg/m^3	1,501	1,401	1,411	1,334	1,352	1,250	1,318
Mixture viscosity at transfer velocity, cP	16.78	9.73	6.24	6.5	4.37	3.91	3.76

5.3 Slurry Pipeline Transfer Assessment Results

The critical velocity and corresponding pressure drop were determined by applying the critical velocity models of Wasp et al. (1977), Oroskar-Turian (1980), and Zandi-Govatos (1967). For the pressure drop, we used the Wasp model (Wasp et al. 1977). These models and application procedures are described in Appendix B. For the critical velocity, the Wasp and Oroskar-Turian models produced very similar results, but the Zandi-Govatos model produced much smaller critical velocity due to its limited applicability to the fine particles. Thus we present the results predicted by the Wasp model for both the critical velocity and pressure drop for the AN-105 slurry transfer to the AP Tank Farm.

Table 5.2 presents the estimated critical velocities and associated pressure drops for the seven cases. The table also includes pipe Reynolds number and vertical uniformity of the solid concentrations. All seven cases have critical velocities of 1.33 to 1.55 ft/sec (0.41 to 0.47 m/s) and a pressure drop of 10 to 23 psi. Associated Reynolds numbers vary from 3,107 to 12,015, all indicating the slurry flow to be in a turbulent flow regime. Furthermore, the slurry transfer would achieve a vertical uniformity of 97.3 to 99.9%, indicating the solid concentrations for all cases are practically homogenous. At these critical velocities, the AN-105 slurry with or without dilution would be transferred without solids settling in the bottom of the pipe during the waste transfer.

The pipeline systems of the AN and AP Tank Farms have maximum pressure capacities of 275 and 400 psi, respectively, which are significantly above the expected pressure drop for these seven cases. Thus, the pipeline system for transferring AN-105 mixed waste slurry to the AP Tank Farm is capable of transferring the waste with and without dilution by water.

At 4.9 and 6 ft/sec (0.71 and 1.8 m/s) slurry transfer velocities, the corresponding pressure drops of the AN-105 WTC from the AN to the AP farm are shown in Table 5.3. Even at 6 ft/sec slurry pipeline velocity, the maximum pressure for all seven cases is 252 psi (for Case 1, no dilution), and does not exceed 275 psi. At 4.9 ft/sec, the maximum pressure drop is less than 200 psi. These estimates indicate that AN-105 can be transferred to the AP Tank Farm within the existing pipeline system at these velocities.

Table 5.2. Estimated Slurry Density, Critical Velocity, and Pressure Drop

Cases	Critical Velocity, ft/sec	Pressure Drop, psi	Reynolds Number	Vertical Uniformity, %
1	1.46	23	3,107	99.5
2	1.52	20	5,252	99.1
3	1.11	10	5,818	99.9
4	1.55	18	7,648	98.5
5	1.33	12	9,658	98.3
6	1.57	15	12,015	97.3
7	1.33	12	10,911	97.9

Table 5.3. Estimated Pressure Drops of the AN-105 WTC Waste

Cases	**Pressure Drop**, psi	
	Slurry Velocity, 4.9 ft/sec	Slurry Velocity, 6.0 ft/sec
1	178	252
2	151	215
3	140	200
4	134	192
5	127	183
6	117	167
7	122	175

6.0 Summary and Conclusions

The study assessed waste retrieval and subsequent pipeline transfer for Tank 241-AN-105 for each of the following steps:

Step 1. Remove supernatant liquid waste from AN-105 and transfer it through a pipeline with inline dilution with water (1^{st} liquid waste transfer).
Step 2. Add water (as a diluent) to Tank AN-105.
Step 3. Mix the saltcake waste and water by mixer pumps to dissolve soluble solids.
Step 4. Let undissolved solids settle to the tank bottom.
Step 5. Remove the resulting supernatant liquid waste from Tank AN-105 (2^{nd} liquid waste transfer).

We also evaluated the AN-105 solid-liquid transfer to AP-102 and AP-104 through a 3-inch (0.07-m) pipeline.

To assess these five waste retrieval steps and the slurry waste pipeline transfer, we conducted rheology measurements and solids identification. We used six AN-105 samples received from the Hanford Site contractor to conduct laboratory rheology measurements at various dilution conditions. These samples were diluted by supernatant liquid, inhibited water, or both to obtain various diluted samples. The shear stress of the sample as a function of shear rate between 5 and 350 s^{-1} was determined using a Bohlin CS rheometer with a C25 geometry.

AN-105 WTC exhibits pseudoplastic behavior with a yield stress of approximately 0.25 Pa. A hysteresis is observed in these measurements, indicating that the composite is also thixotropic. These rheology data were fit to a yield power law model, while the settled supernatant from the three different dilutions exhibited Newtonian behavior. The settled solids exhibit yield strength of up to 100 Pa and viscosity of up to 170 cP (0.17 pa-s).

The first measurement made on the supernatant dilution indicated that the material had gel-like properties with a yield stress of 34.6 Pa. After the material yielded, the shear stress continued to drop with increasing shear rate and the material exhibited yield pseudoplastic behavior with a much lower yield stress (0.45 to 0.05 mPa). The duplicate sample did not display this same behavior but appeared to exhibit Bingham plastic properties. Bingham plastics require a minimum amount of stress before deformation but then exhibit linear increases in shear stress as a function of shear rate.

Both the water dilution and supernatant plus water dilution exhibited Newtonian behavior with viscosities similar to those observed by the settled supernatants for these dilutions. The solids in these dilutions settle quickly, making it difficult to obtain accurate viscosities of the suspended solutions, and may have contributed to measuring viscosities similar to those obtained for the settled liquid.

By combining in situ rheology data measured by ball rheometers (Stewart et al. 1996), Herting's data (1997), and these current data, we developed the AN-105 specific viscosity model, changing from several centipoise for a diluted supernatant liquid to 20 million cP for saltcake (at very

small strain rates of about 0.001 s^{-1}) as a function of strain rate and solid concentration. This viscosity model was implemented to the TEMPEST code to conduct the pump jet mixing.

Prior to this study, there were no direct measurements to identify solids in the AN-105 waste. Therefore, we evaluated the crystallinity, morphology, chemical composition, and crystal phases of AN-105 saltcake samples with BF, SAD, and EDS. These measurements show the chemical elements Na, O, Si, Al, Mg, Cl, S, K, P, Cr, and Sr in decreasing order. These chemical evaluations identified magnesium silicate (possibly $Mg_8Si1_2O_{32}\cdot 4H_2O$, SiO2), aluminum silicate, sodium aluminum silicate, calcium hydroxide, magnesium hydroxide, potassium silicate (possibly $K_2Si_2O_5$), sodium hydroxide hydrate (possibly $NaOH\cdot H_2O$), and sodium nitrate [possibly $Na_3O(NO_2)$]. The solid identified as sodium nitrate may be thermonatrite ($Na_2CO_3\cdot H_2O$). Also depending on the interpretation of the EDS measurement, there may be thenardite (Na_2SO_4) in the AN-105 saltcake sample. These measurements did not detect gibbsite [$Al(OH)_3(s)$], even through it is commonly believed that AN-105 saltcake contains gibbsite.

For the first waste transfer (Step 1 above), we assigned that the AN-105 supernatant liquid would be diluted by water at the ratio of 1 volume liquid waste to 0.56 volume water. Chemical modeling indicates that the main aqueous chemical species of the supernatant liquid [Na+, CO_3^{2-}, SO_4^{2-}, OH^-, NO_3^-, $NaNO_3(aq)$, NO_2^-, $NaNO_2(aq)$, $Al(OH)_4^-$, Cl^-, $Cr(OH)_4^-$, $H_2SiO_4^{2-}$] are in equilibrium conditions with solids consisting mainly of $NaCO_3\cdot H_2O(s)$, $NaSO_4(s)$, $Cr(OH)_3(s)$, and $Ca(OH)_3$ in AN-105 saltcake. With 56 vol% dilution of the AN-105 supernatant liquid with water, the model predicted that most of the aqueous chemical concentrations were reduced, including the OH^- concentration. The reduced OH^- concentration resulted in precipitation of gibbsite, which in turn made the OH^- concentration increase again slightly. However, the amount of precipitated gibbsite would only be about 0.3 molality. With this dilution, 0.003 molality of chromium hydroxide [$Cr(OH)_3$] was also precipitated from the diluted AN-105 supernatant liquid waste. No other solids were precipitated from this inline dilution.

Our BF, EDS, and SAD measurements of AN-105 saltcake did not detect gibbsite. Herting (1997) did not report formation of gibbsite due to dilution of AN-105 WTC waste or saltcake during his dilution experiments. Thus, in spite of the chemical model's prediction of gibbsite, it is possible that gibbsite would not precipitate under this inline dilution condition. But assuming that gibbsite does precipitate, the precipitation would produce about 75 tons of gibbsite and a very small amount of chromium hydroxide. This results in 0.6 vol% solids (density 2,420 kg/m^3) being transferred through the pipeline.

With 0.6 vol% of gibbsite (having a particle density of 2,420 kg/m^3) in the diluted AN-105 waste, we estimated that the critical velocity of the waste would be approximately 0.3 m/s (1 ft/sec) to maintain a turbulent pipe flow. Thus, there would be no solids deposition in the pipeline when the expected slurry pipeline velocity is about 1.2–1.8 m/s (4–6 ft/sec) (Julyk et al. 2002). Although at the early stage of the gibbsite formation solids may be sticky, gibbsite precipitation may be too slow (probably days to weeks) to be of concern during the waste pipeline transfer.

These evaluations indicate that there would be no adverse impact on the AN-105 supernatant liquid properties that hinder waste pipeline transfer due to inline dilution of AN-105 supernatant liquid waste with water.

After the supernatant liquid has been removed from Tank AN-105 with inline dilution, the remaining saltcake waste would be diluted by 79% with water in the tank (Steps 2 and 3 above). After confirming the reasonableness of our chemical model predictions with Herting's AN-105 experimental data, we simulated chemical reactions due to saltcake dilution by water. The AN-105 dilution model predicts that all $Na_2CO_3 \cdot H_2O(s)$ and $Na_2SO_4(s)$ would be dissolved. Only small amounts of $Cr(OH)_3(am)$ and $Ca(OH)_2(s)$ and possibly sodium oxalate [$Na_2C_2O_4(s)$], would remain as solids. The expected waste volume reduction is over 90%. The remaining solids [$Cr(OH)_3(am)$, $Ca(OH)_2(s)$, and possibly $Na_2C_2O_4(s)$] are expected to settle without forming a gel (Step 4), and would be separated from the supernatant liquid. Thus, it is feasible to retrieve the resulting supernatant liquid from 79% in-tank dilution of saltcake and to transfer it through the 3-inch (0.07-m) pipeline.

To assess Step 4, we evaluated how effective two 20-ft- (6.1 m) off-center, 300-hp mixer pumps would be for mixing AN-105 waste when the AN-105 saltcake is mixed with water at a ratio of 1 volume saltcake to 0.79 volume water. We used the TEMPEST code to simulate mixing the saltcake and water with the pumps. We did not reduce the saltcake volume and initial yield strength in the AN-105 model, so we achieved a conservative assessment, even though the chemical modeling discussed above indicated that over 90 vol% of saltcake would be dissolved by water. The model predicted that, after 30 minutes of mixing, mixer pumps would mobilize all the solids, and the solids would be fully mixed over the entire tank. Thus, two 300-hp mixer pumps would erode all AN-105 saltcake and distribute it uniformly over the entire tank even under the conservative conditions imposed in this evaluation.

We also evaluated solid-liquid waste slurry transfer from Tank AN-105 to Tanks AP-102 and AP-104 through a 3-inch-diameter pipeline for a distance of 0.7 mile. We selected seven cases based on slurry transfer criteria. These cases consider transfer of AN-105 fully mixed waste without dilution and with 25%, 50%, and 100% dilution with and without accounting for solids dissolution. These cases have slurry densities that vary from 1.25 to 1.5 g/mL. For all seven cases the critical velocities are estimated as 1.33 to 1.55 ft/sec (0.41 to 0.47 m/s), and associated pressure drops are 10 to 23 psi. The slurry transfer would achieve 97.3 to 99.9% vertical uniformity, indicating that solid concentrations are homogeneous. At 4.9 ft/s (0.71 m/s) and 6 ft/sec (1.8 m/s) transfer velocities, the pressure drops for waste without dilution are 178 and 275 psi. The AN-105 waste slurry with dilution requires less pressure drop. Thus the AN-105 waste can be transferred to the AP Tank Farm through the existing 3-inch pipeline system at these velocities.

This AN-105 waste assessment concludes that the AN-105 waste can be retrieved with inline and in-tank dilution and can be transferred through a 3-inch (0.07-m) pipeline, including the slurry transfer to AP-102 and AP-104, under the waste and mixing conditions used in this assessment.

7.0 References

Felmy AR. 1995. "GMIN: A Computerized Chemical Equilibrium Program Using a Constrained Minimization of the Gibbs Free Energy: Summary Report." *Chemical Equilibrium and Reaction Models*, Solid Science Society of America, Special Publication 42.

Herting DL. 1997. *Results of Dilution Studies with Waste from Tank 241-AN-105*. HNF-SD-WM-DTR-046 Rev. 0, Numatec Hanford Corp. Richland, WA.

Herting DL. 1998. *Results of Dilution Studies with Waste from Tank 241-AN-104*. HNF-3352, Rev. 0, Numatec Hanford Corp. Richland, WA.

Jo J, LW Shelton Jr, TL Welch, and J Stroup. 1997. *Tank Characterization Report for Double-Shell Tank 241-AN-105*. HNF-SD-WM-ER-678 Rev. 0, Richland, WA.

Julyk LA, TC Oten, and WL Willis. 2002. *Waste Feed Delivery Transfer System Analysis*. RPP-5346 Rev. 2, CH2M HILL Hanford Group, Inc., Richland, WA.

Onishi Y and KP Recknagle. 1998. *Performance Evaluation of Rotating Pump Jet Mixing of Radioactive Wastes in Hanford Tanks 241-AP-102 and –104*. PNNL-11920, Pacific Northwest National Laboratory, Richland, WA.

Onishi Y and DS Trent. March 1999. "Mobilization Modeling of Erosion-Resisting Radioactive Tank Waste." *Proceedings of the Rheology in the Mineral Industry II*, Kahuku, Oahu, Hawaii. United Engineering Foundation, New York, pp. 45-56.

Onishi Y, BE Wells, SA Hartley, and SK Cooley. 2002. *Pipeline Cross-Site Transfer Assessment for Tank 241-SY-101*. PNNL-13650, Pacific Northwest National Laboratory, Richland, WA.

Onishi Y, ST Yokuda, and CH Majumder. 2002. *Optimal Elevation and Configuration of Hanford's Double-Shell Tank Waste Mixer Pumps*. PNNL-13913, Pacific Northwest National Laboratory, Richland, Washington.

Orme RM, DJ Geniesse, and GT MacLean. 2001. *Generalized Feed Delivery Descriptions and Tank-Specific Flowsheets.* RPP-8218 Rev. 0, CH2M HILL Hanford Group, Inc., Richland, WA.

Oroskar AR and RM Turian. 1980. "The Critical Velocity in Pipeline Flow of Slurries." *AIChE Journal*, Vol. 26, No. 4.

Shekarriz A, DR Rector, LA Mahoney, MA Chieda, JM Bates, RE Bauer, NS Cannon, BE Hey, CG Linschooten, FJ Reitz, and ER Siciliano. 1997. *Composition and Quantities of Retained Gas Measured in Hanford Waste Tanks 241-AW-101, A-101, AN-105, AN-104, and AN-103*. PNNL-11450, Pacific Northwest National Laboratory, Richland, WA.

Stewart CW, JM Alzheimer, ME Brewster, G Chen, RE Mendoza, HC Reid, CL Shepard, and G Terrones. 1996. *In Situ Rheology and Gas Volume in Hanford Double-Shell Waste Tanks*. PNNL-11296, Pacific Northwest National Laboratory, Richland, WA.

Trent DS and LL Eyler. 1993. *TEMPEST: A Computer Program for Three-Dimensional, Time-Dependent Computational Fluid Dynamics.* PNL-8857 Vol. 1, Pacific Northwest National Laboratory, Richland, WA.

Wani CA. 1982. "Critical Velocities in Multisize Particle Transportation Through Horizontal Pipes." *Journal of Pipelines*, Vol. 2, pp. 57-62.

Wasp EJ. 1977. *Solid-Liquid Flow Slurry Pipeline Transportation*. Trans Tech Publications.

Wells BE, JM Cuta, SA Hartley, LA Mahoney, PA Meyer, and CW Stewart. 2002. *Analysis of Induced Gas Releases During Retrieval of Hanford Double-Shell Tank Waste*. PNNL-13782 Rev. 1, Pacific Northwest National Laboratory, Richland, WA.

Zandi I and G Govatos. 1967. "Heterogeneous Flow of Solids in Pipelines." *J. Hydr. Div.* ASCE, 93:HY3, Prod. Paper 5244, pp. 145-159.

Appendix A

Solid Phase Characterization

Appendix A
Solid Phase Characterization

Prior to this study, there were no direct measurements to identify solids in the AN-105 waste. Thus, we evaluated the crystallinity, morphology, chemical composition, and crystal phases of AN-105 saltcake samples with bright field image (BF), select area diffraction (SAD), and energy dispersive x-ray spectroscopy (EDS). The experimental condition was at 120 kV high tension. The magnification was up to 100KX, and the space resolution was up to 50 nm.

A.1 Overall Composition

EDS results in Figure A.1(a) and A.1(b) reveal the elements of Na, O, Si, Mg, Cl, S, K, P, Cr, and Sr in decreasing order in a low magnification area of the sample shown in Figure A.2 taken by BF.

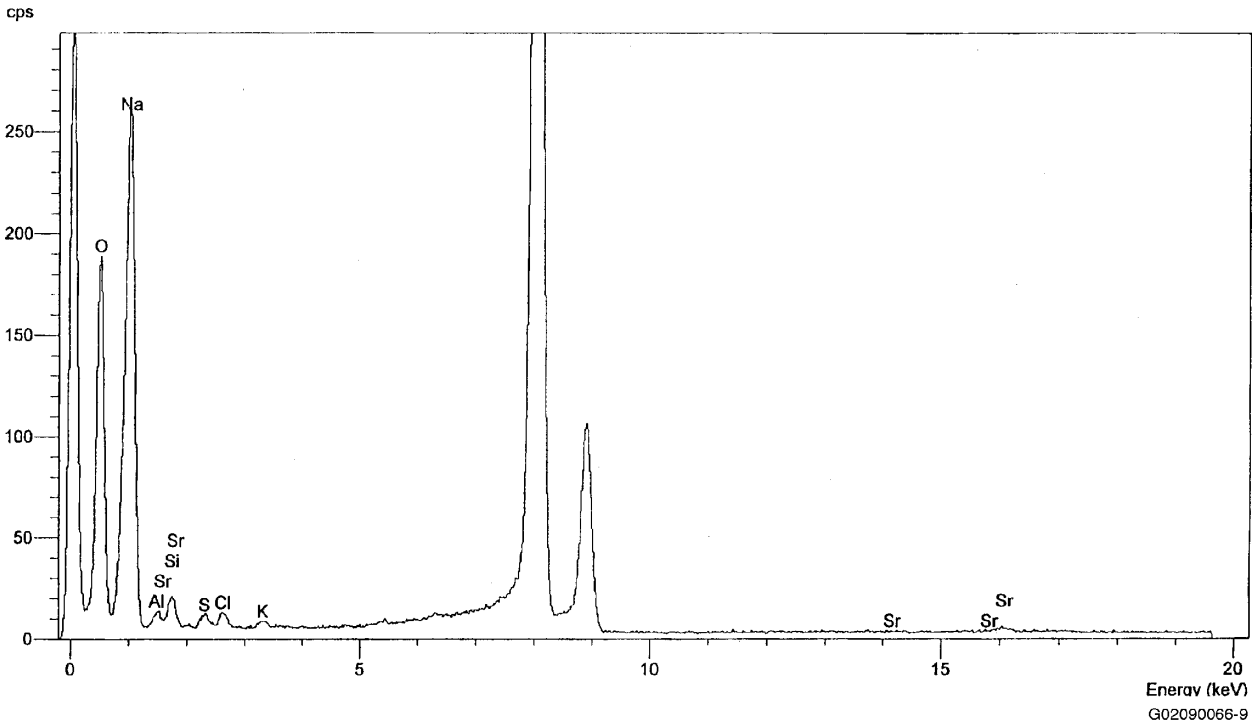

Figure A.1(a). EDS Measurement

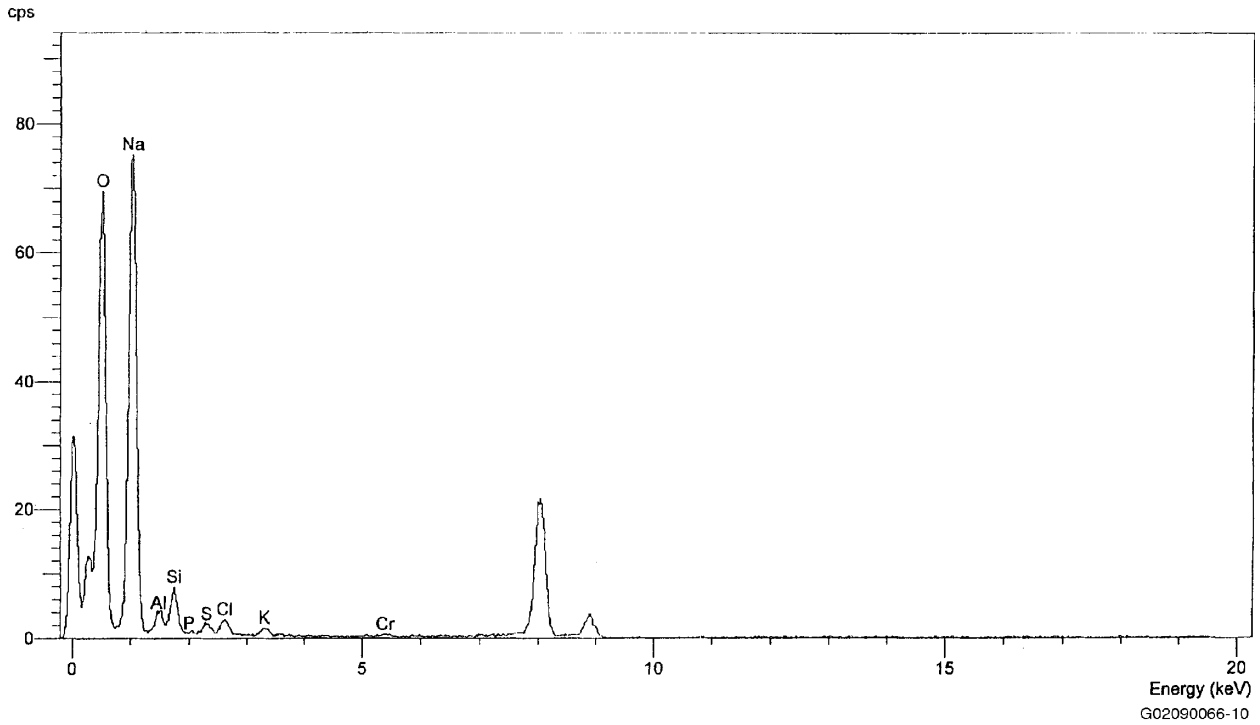

Figure A.1(b). EDS Measurement

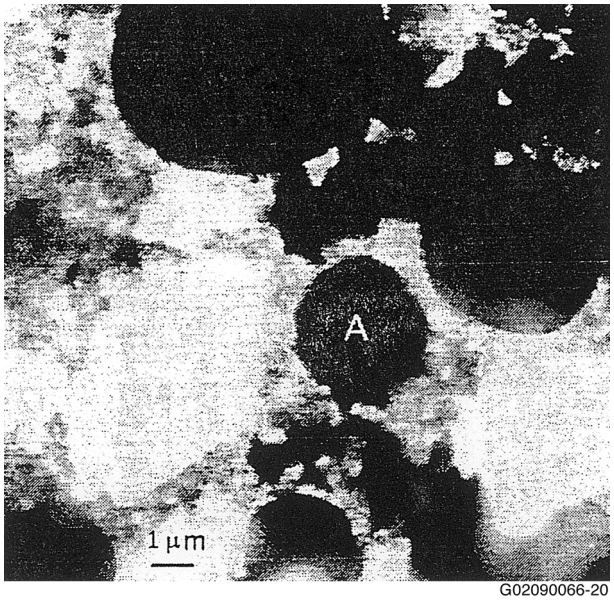

Figure A.2. Bright Filed Image Showing $NaOH \cdot H_2O$

A.2 Solid Phase Identification

The following solids were identified:

- Sodium hydroxide hydrate ($NaOH \cdot H_2O$): The BF image shown in Figure A.2 identified Particle A as sodium hydroxide hydrate as stated above. It is also shown in Area A of the BF image (Figure A.2), and an EDS measurement (Figure A.3). The EDS measurement could be interpreted to have sodium sulfate (possibly Na_2SO_4)

- Magnesium silicate, (possibly $Mg_8Si1_2O_{32} \cdot 4H_2O$, SiO2): This solid was identified as Particles A and F of a BF image (Figure A.4), Particle D of a BF image (Figure A.5), a SAD image (Figure A.6), and an EDS measurement (Figure A.7).

- Silica, SiO2: This solid is reveals as Particle B of the BF image (Figure A.4) and an EDS measurement (Figure A.8).

- Aluminum silicate: It is shown as Particle C of the BF image (Figure A.4), a SAD image (Figure A.9), and an EDS measurement (Figure A.10).

- Sodium aluminum silicate: It is shown as Particle D of the BF image (Figure A.4), Particle A of the BF image (Figure A.5), a SAD image (Figure A.11), and an EDS measurement (Figure A.12).

- Calcium hydroxide: It appears as Particle E of the BF image (Figure A.4), SAD image (Figure A.13), and EDS measurement (Figure A.14).

- Magnesium hydroxide: It is shown as Particle B and C of the BF image (Figure A.5), and an EDS measurement (Figure A.15).

- Potassium silicate (possibly $K_2Si_2O_5$) and sodium hydroxide hydrate (possibly $NaOH \cdot H_2O$): Area A of a BF image (Figure A.16), a SAD image (Figure A.17), and an EDS measurement (Figure A.18).

- Sodium Nitrate [possibly $Na_3O(NO_2)$]: It is shown in Area A of a BF image (Figure A.19), a SAD image (Figure A.20), and an EDS measurement (Figure A.21). However, the solid could be sodium carbonate (possibly $Na_2CO_3 \cdot H_2O$).

Thus, these BF, SAD and EDS measurements identified sodium hydroxide hydrate (possibly $NaOH \cdot H_2O$), magnesium silicate (possibly $Mg_8Si1_2O_{32} \cdot 4H_2O$, SiO2), aluminum silicate, sodium aluminum silicate, calcium hydroxide, magnesium hydroxide, potassium silicate (possibly $K_2Si_2O_5$), and sodium hydroxide hydrate (possibly $NaOH \cdot H_2O$), and sodium nitrate [possibly Na3O(NO2)]. However, the solid identified as sodium nitrate may be thermonatrite ($Na_2CO_3 \cdot H_2O$). Also depending on the interpretation of the EDS measurement, there may also be thenardite (Na_2SO_4) in the AN-105 saltcake sample. It is commonly believed that AN-105 saltcake contains gibbsite [Al(OH)3(s)] as aluminum solid. However, even with repeated attempts to find gibbsite, these measurements did not detect it in the AN-105 saltcake samples.

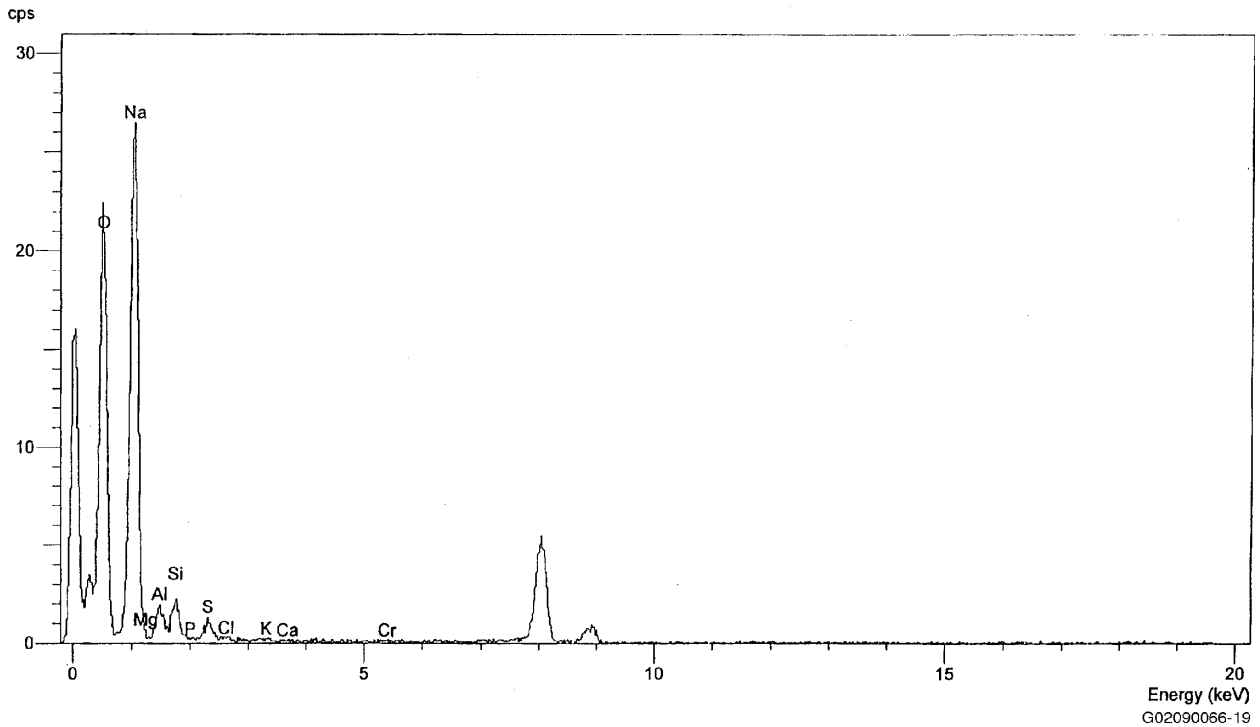

Figure A.3. EDS Measurement Indicating Sodium Hydroxide Hydrate (or possibly sodium sulfate)

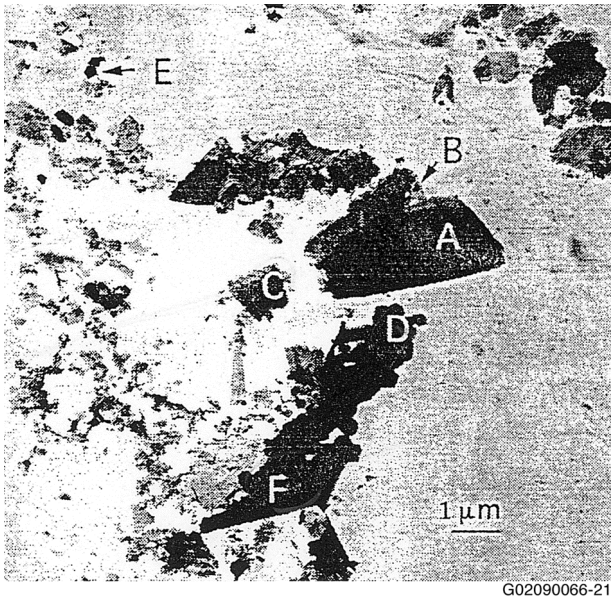

Figure A.4. Bright Filed Image Revealing Magnesium Silicate, Silica, Aluminum Silicate, Sodium Aluminum Silicate, and Calcium Hydroxide

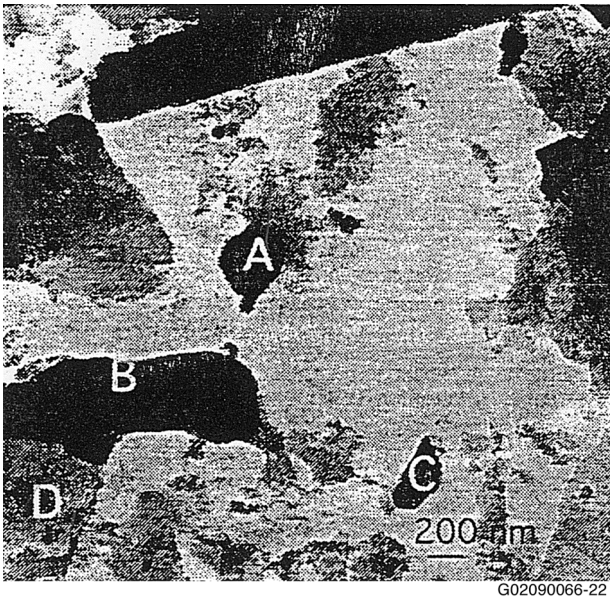

Figure A.5. Bright Filed Image Revealing Magnesium Silicate, Sodium Aluminum Silicate, and Magnesium Hydroxide

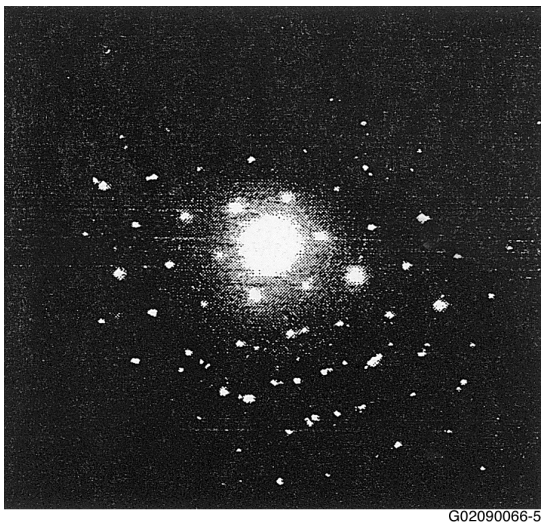

Figure A.6. Select Area Diffraction Image Showing Magnesium Silicate

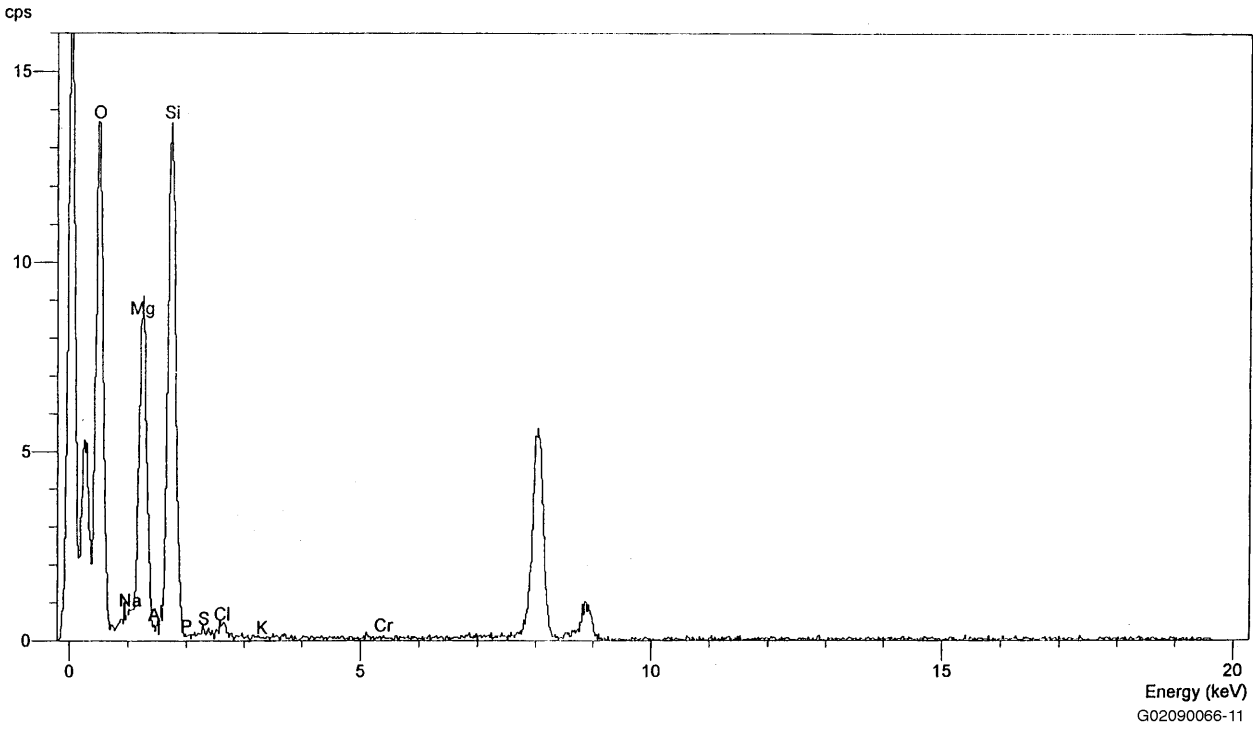

Figure A.7. EDS Measurement Indicating Magnesium Silicate

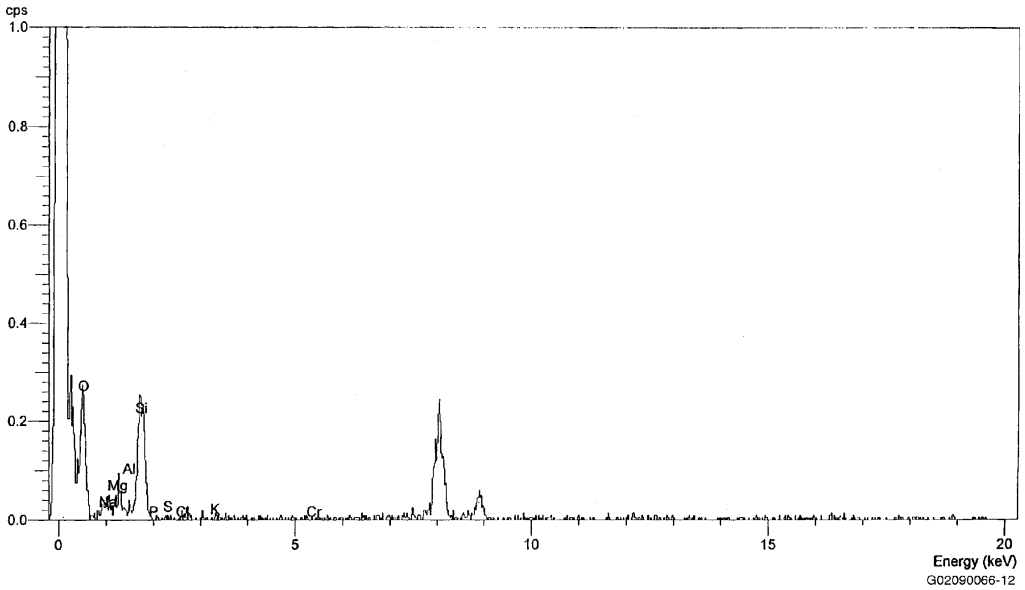

Figure A.8. EDS Measurement Indicating Silica

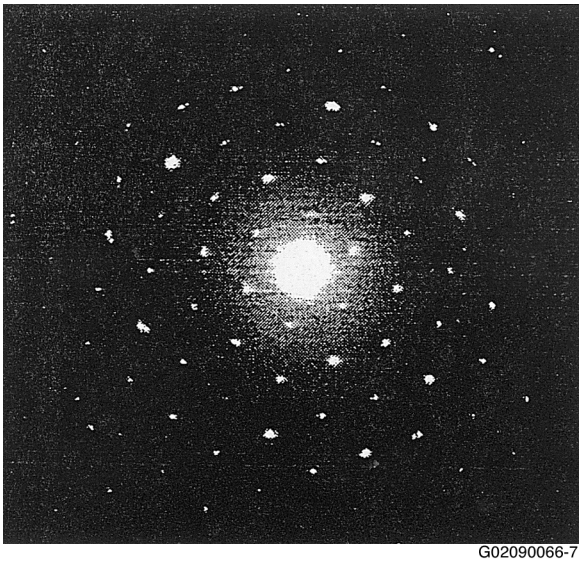

Figure A.9. Select Area Diffraction Image Showing Aluminum Silicate

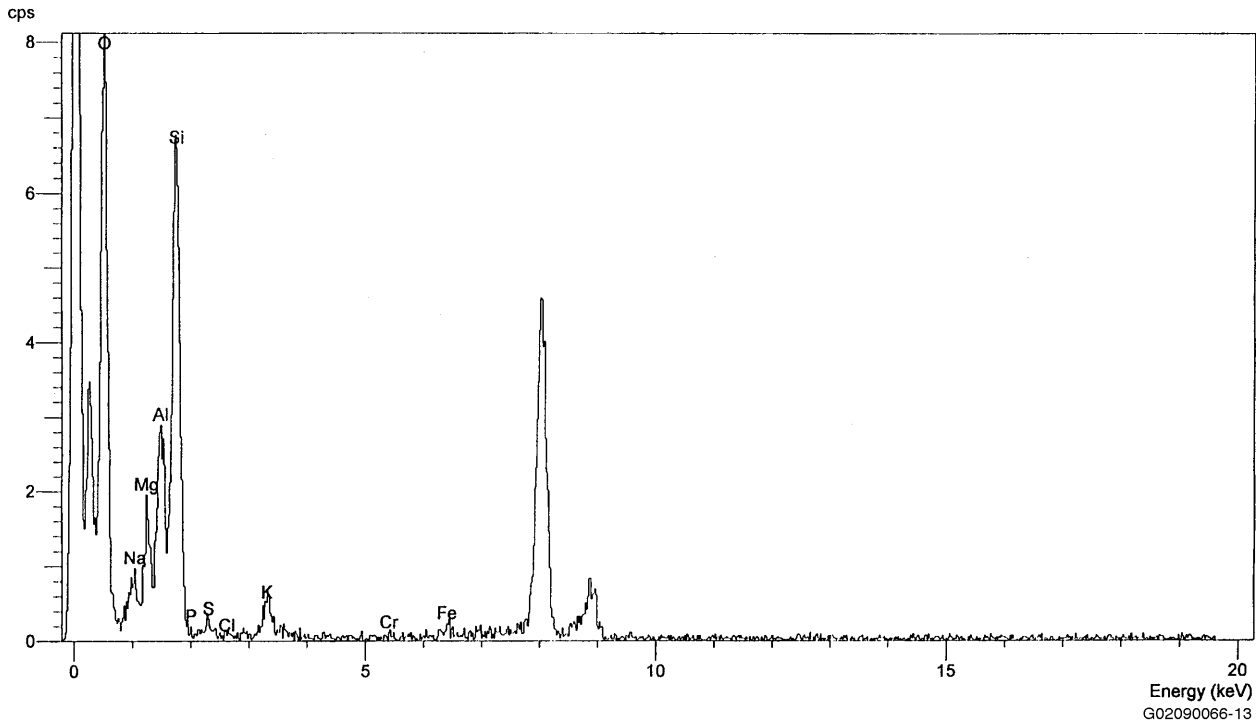

Figure A.10. EDS Measurement Indicating Aluminum Silicate

Figure A.11. Select Area Diffraction Image Showing Sodium Aluminum Silicate

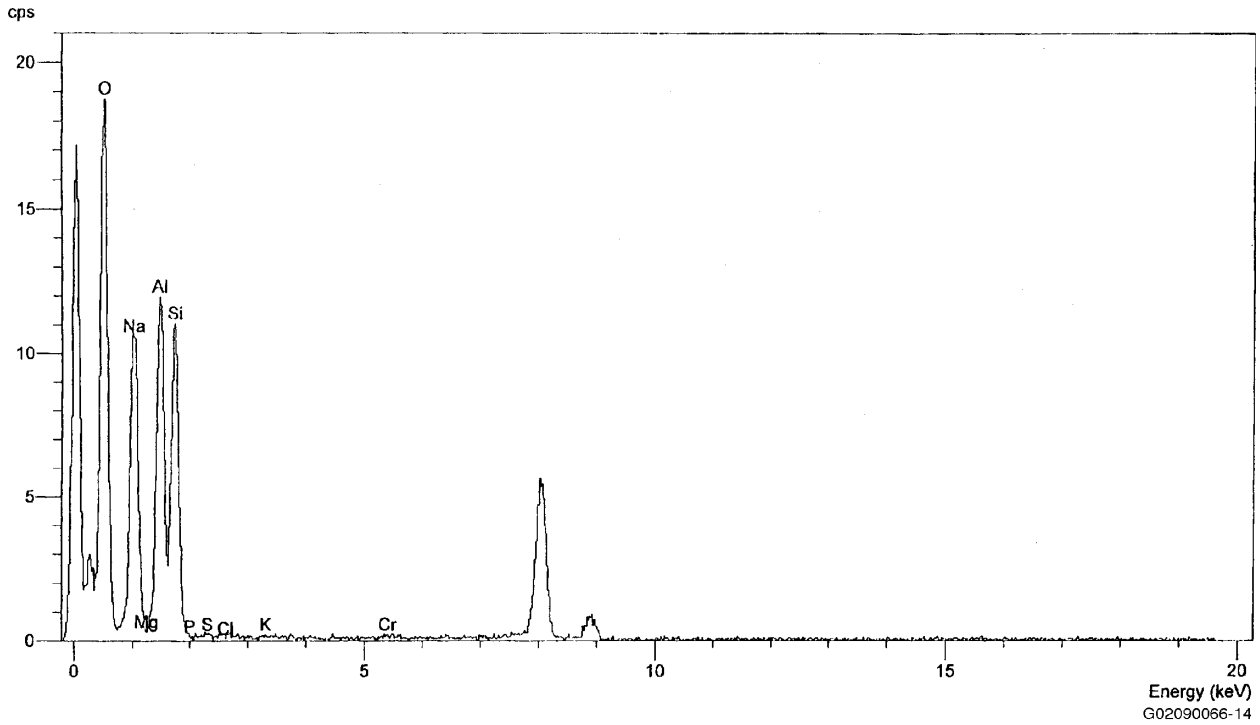

Figure A.12. EDS Measurement Indicating Sodium Aluminum Silicate

Figure A.13. Select Area Diffraction Image Showing Calcium Hydroxide

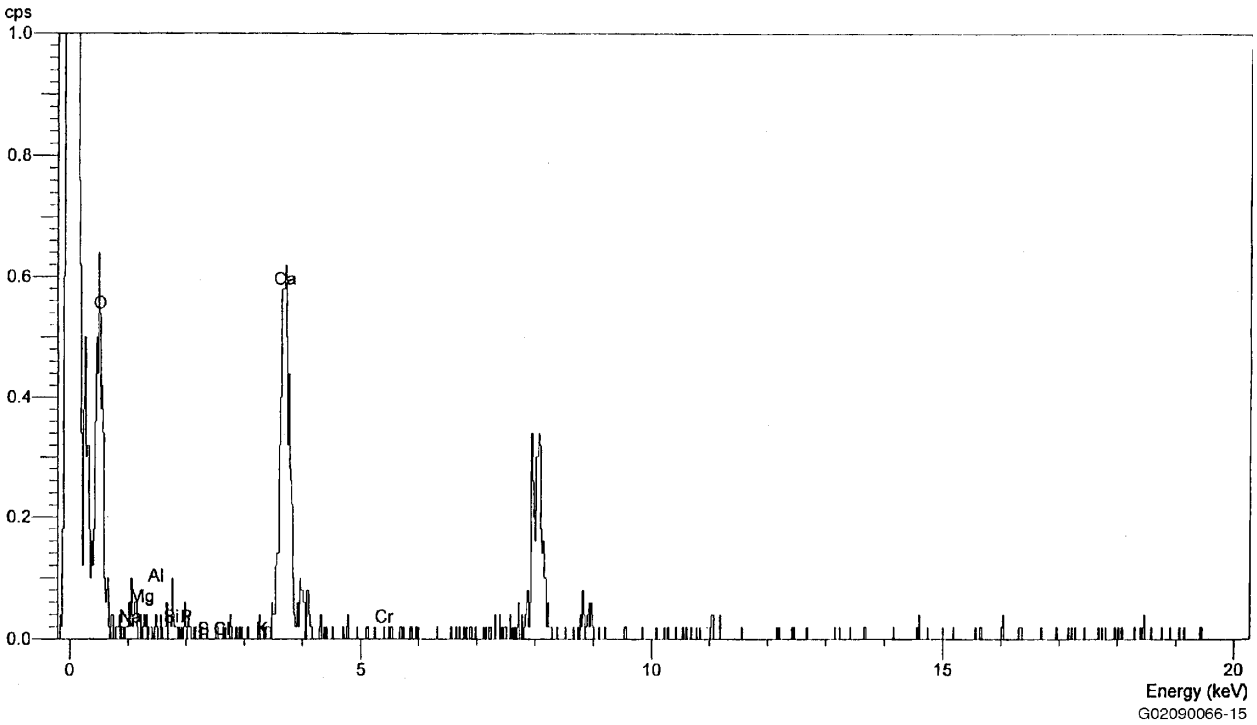

Figure A.14. EDS Measurement Indicating Calcium Hydroxide

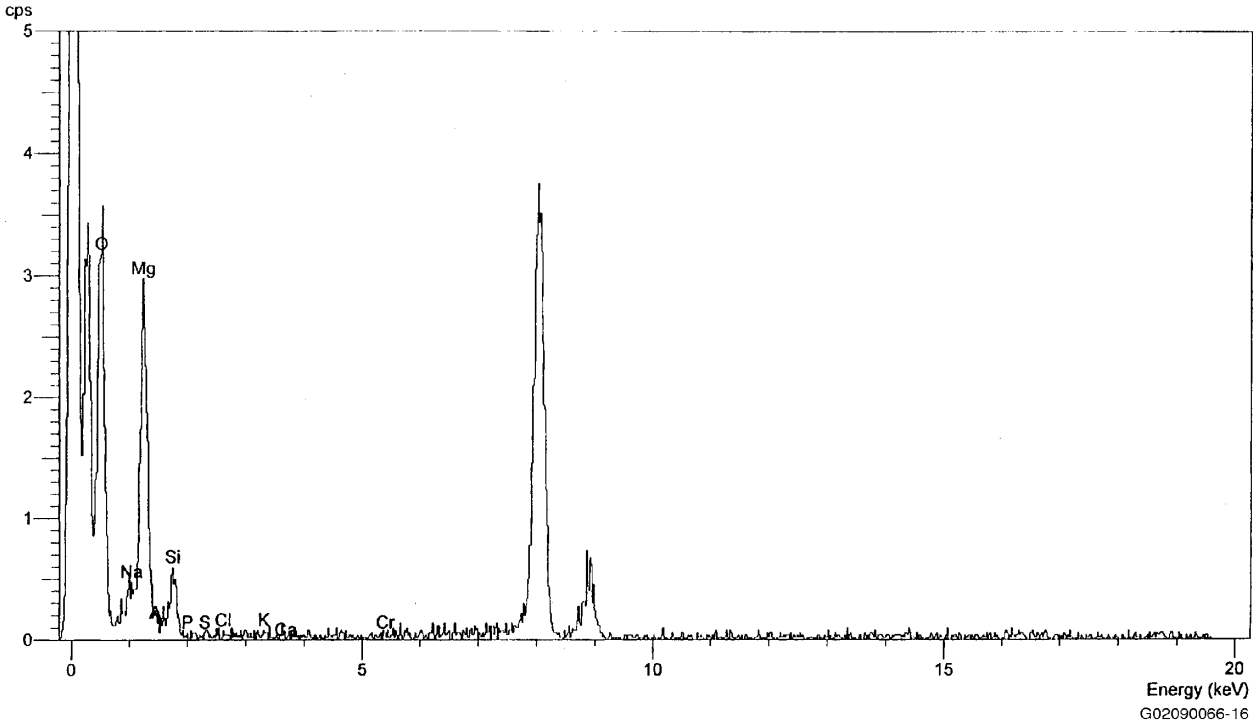

Figure A.15. EDS Measurement Indicating Magnesium Hydroxide

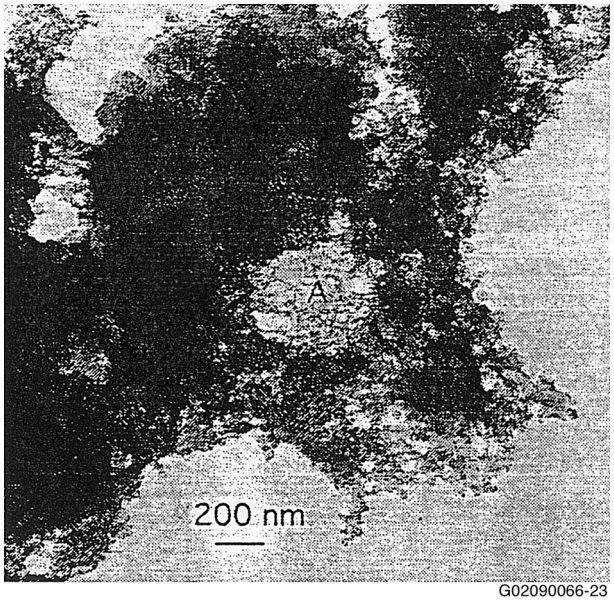

Figure A.16. Bright Filed Image Revealing Magnesium Silicate, Sodium Aluminum Silicate, and Magnesium Hydroxide

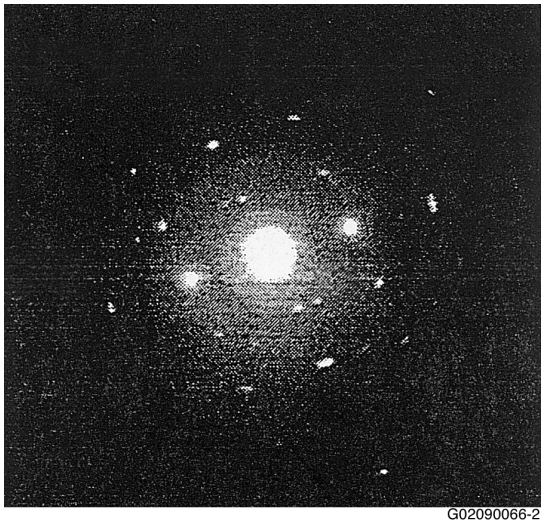

Figure A.17. Select Area Diffraction Image Showing Potassium Silicate and Sodium Hydroxide Hydrate

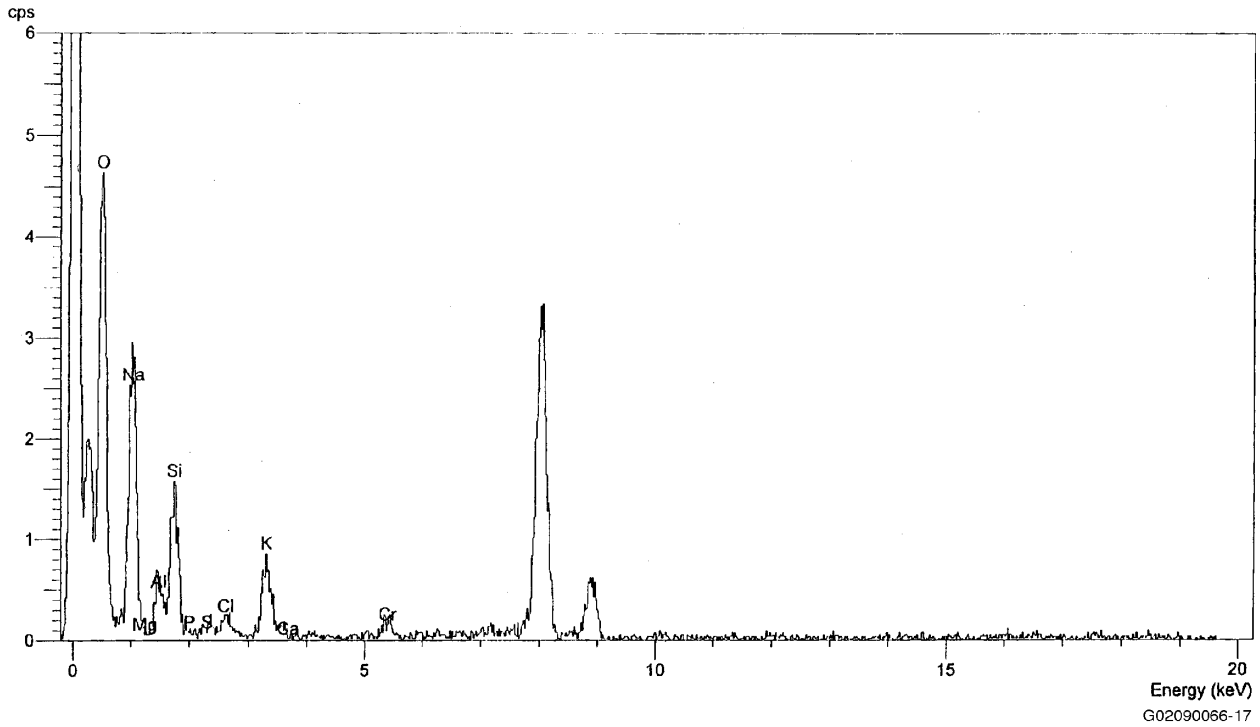

Figure A.18. EDS Measurement Indicating Potassium Silicate and Sodium Hydroxide Hydrate

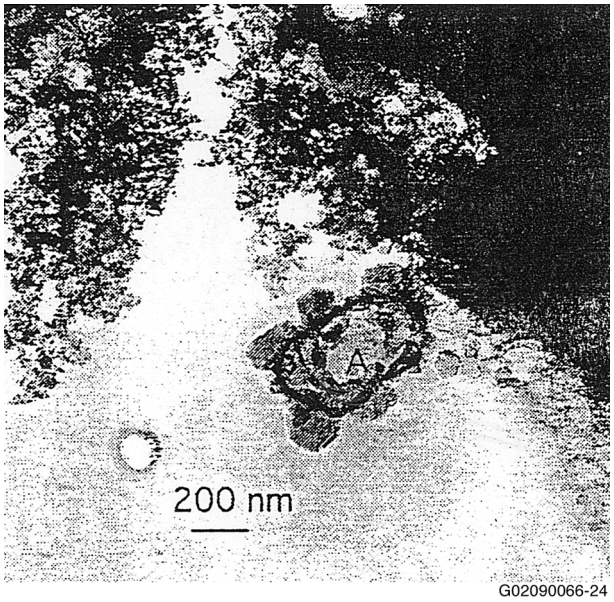

Figure A.19. Bright Filed Image Revealing Magnesium Silicate, Sodium Aluminum Silicate, and Magnesium Hydroxide

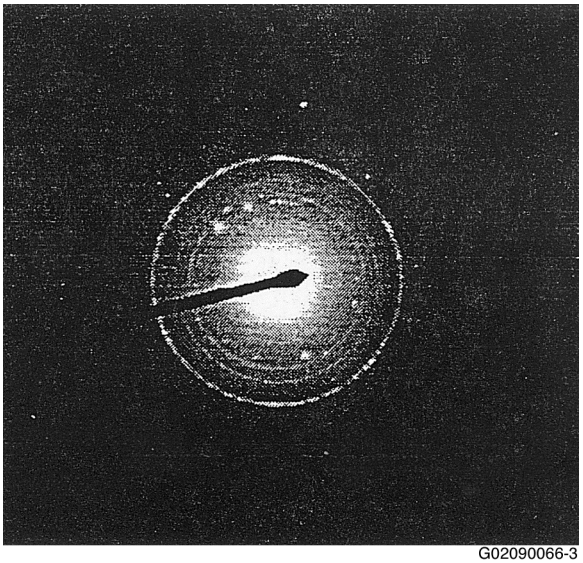

Figure A.20. Select Area Diffraction Image Showing Sodium Nitrate

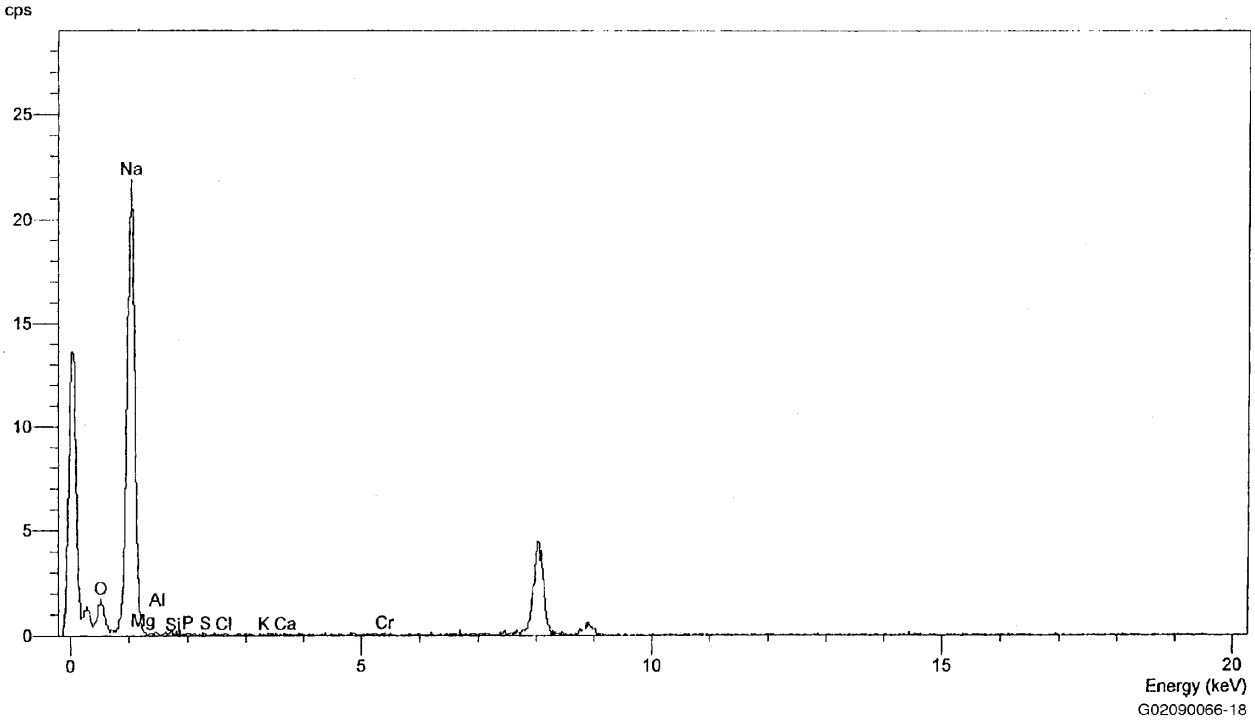

Figure A.21. EDS Measurement Indicating Sodium Nitrate (or possibly sodium carbonate)

Appendix B

Slurry Pipeline Transfer Assessment Methodologies

Appendix B
Slurry Pipeline Transfer Assessment Methodologies

B.1 Slurry Pipeline Transfer

When transporting solid-liquid slurry through a horizontal pipeline, the flow must have enough kinetic and turbulent energy to maintain the particles in suspension and avoid the formation of a stationary bed at the bottom of the pipe. The critical velocity is the bulk average flow velocity above which full particulate suspension is maintained and the pipeline discharge pressure is stable. The slurry may exhibit a range of behavior from homogeneous to heterogeneous flow.

The homogeneous and heterogeneous flows bound the behaviors of solid-liquid slurry flow. Heterogeneous flows are those in which the solids are not uniformly distributed along the vertical axis of a horizontal pipe. Slurries exhibiting heterogeneous behavior commonly have "coarse" solid particle sizes such that the effect of particle settling and inertia are significant—the liquid and solid phases, although mixed, remain as separate entities. The coarse solids do not have a large effect on the liquid properties; hence, the increase in system viscosity is usually small. As a result of the significant particle inertia and settling effects in these slurries, a substantial amount of turbulent energy is required to maintain particle suspension. Subsequently, the critical deposition velocity is large enough that in general the flow is fully turbulent. These heterogeneous slurry systems are referred to as "deposition limited."

Slurries exhibiting homogeneous behavior commonly have fine solid particle sizes such that the effect of particle settling and inertia are minor. The fine solids become uniformly distributed throughout the carrier fluid, modifying the fluid properties. Usually the viscosity is increased compared to that of the base fluid. Some systems, especially those with high solids concentrations, exhibit non-Newtonian rheology. For these non-Newtonian cases a suitable rheology model must be used to accurately characterize the flow. Because particle settling and inertia effects are small, only a small amount of turbulent energy may be required to maintain particle suspension, and the deposition velocity is typically small such that the flow may be laminar. When transferring truly homogeneous slurry the pipeline pressure may be stable for a laminar flow condition. However, real slurry will have slight amounts of heterogeneous particles that could possibly form stationery or sliding beds that cause pressure instabilities. To ensure a stable system, the critical velocity should be increased such that the system has made the transition from laminar to turbulent flow. These homogeneous slurry systems are referred to as "transition limited."

B.2 Critical Velocity

B.2.1 Wasp's Method

For estimation of the critical velocity for the transport of AN-105 waste we use Wasp's method (Wasp 1977). Wasp modified Durand's relation (Durand 1953) to adequately represent the effect of particle concentration and mean particle diameter. The resulting correlation gives the critical velocity as

$$U_c = 3.116 C_v^{0.186} \left[2gD\left(\frac{\rho_s - \rho_l}{\rho_l} \right) \right]^{\frac{1}{2}} \left(\frac{d}{D} \right)^{\frac{1}{6}} \tag{B.1}$$

In the above relation C_v is the total particle volume fraction, ρ_l and ρ_s are the liquid and solid densities, D is the pipe diameter, and d is the particle diameter. This method is applicable to systems with mixed particle sizes using the weighted mean particle diameter. If the result of the calculation were to yield a laminar flow condition (i.e., pipe Reynolds number less than 2300), this would indicate that the slurry is transition limited, and the critical velocity would be increased such that the flow would become fully turbulent (e.g., Re_p = 3000). We have found this a sound method for estimating the critical velocity.

B.2.2 The Method of Oroskar and Turian

A correlation developed by Oroskar and Turian (1980) incorporated the earlier work of several authors and accounted for dissipation of turbulent energy. The critical velocity is calculated by

$$\frac{U_c}{\sqrt{gd(S-1)}} = \left\{ 5 C_v (1 - C_v)^{2n-1} \left(\frac{D}{d} \right) \left(\frac{D \rho_l \sqrt{gd(S-1)}}{\mu} \right)^{1/8} \frac{1}{x} \right\}^{8/15} \tag{B.2}$$

or after regress ional analysis on 357 data points, they present the correlation as

$$\frac{U_c}{\sqrt{gd(S-1)}} = 1.85 C_v^{0.1536} (1 - C_v)^{0.3564} \left(\frac{D}{d} \right)^{0.378} Re_p^{0.09} x^{0.3} \tag{B.3}$$

Here, x is the correction factor for dissipation of turbulent energy, which can be written as follows:

$$x = \frac{4}{\pi} \gamma \exp\left(\frac{-4\gamma^2}{\pi} \right) + \frac{\sqrt{\pi}}{2} \operatorname{erfc}\left(\frac{2\gamma}{\sqrt{\pi}} \right) \tag{B.4}$$

In this relation γ is the ratio of particle settling velocity to critical velocity. In the calculations, x is determined for a range of values for γ. For the settling velocities we've observed and for a

reasonable range of critical velocities (0.02 to 1.62 m/s), the value of x is roughly 0.96. This method gives similar but generally slightly higher values than the Wasp method.

B.2.3 The Method of Zandi and Govatos

Zandi and Govatos (1967) proposed the following analytical correlation for critical velocity:

$$U_c = \sqrt{\frac{40 C_v D g (S-1)}{\sqrt{C_D}}} \tag{B.5}$$

where S is the ratio of solids density to fluid density, C_v is the solids volume fraction, D is the pipeline diameter, and C_D is the particle drag. For large particle sizes in water, this relation gives values that are similar to those of Durand (1953). For small particle sizes, the critical velocity is significantly underpredicted due to the very large particle drag coefficient associated with the small particles.

B.2.4 Wani's Method

Wani et al. (1982) developed a correlation model for slurries in which the particle settling is in the Stokes regime (i.e., particle Reynolds number, Re_p<0.1). The critical velocity is given as

$$\frac{U_c}{gd(S-1)} = 2.3E-4\, Re_p^{0.27} \left(\frac{100}{d}\right)^{0.973} C^{1.67} C_v^{0.307} \tag{B.6}$$

where Re_p is the Reynolds number, defined as

$$Re_p = \frac{\rho_L D \sqrt{gd(S-1)}}{\mu_L}$$

and d is the weighted mean particle diameter, C is the Hazen-William pipe roughness factor, and C_v the solids volume fraction. Wani's method is heavily dependent on the pipe roughness, which makes it unreliable for our applications. The methods of Zandi and Govatos and Wani, while suitable for larger particulate slurries, are not suitable for the fine particulate slurries of the Tank AN-105 waste.

B.3 Pressure Drop Calculation Method

We selected Wasp's method for calculating the pipeline pressure drop (Wasp 1963, 1977). The method was intended for use in a homogeneous-heterogeneous system with multiple particle size fractions. Wasp based his method on the concept of the "two-phase vehicle." Fine particles join with the carrier liquid to form a homogeneous "vehicle," while the coarse particles are suspended as a heterogeneous "bed" in this vehicle. The fine particles in the vehicle modify the flow density and rheology. In fact, the capacity to move and suspend the coarse solids increases with increasing concentration of fine particles in the vehicle.

Central to the method is the determination of the vehicle. The vehicle is based on the homogeneity of the solids concentration. Wasp considers a flow to be homogeneous when the solids concentration (C) at distance y = 0.08D from the top of the pipe is at least 80% of that at the pipe centerline (C_A). From experimental data (Ismail 1952) for the particular cases of y = 0.08D and y = 0.92D, Wasp gives the relationship for these two solid concentrations as

$$\log_{10}\frac{C}{C_A} = \left(\frac{-1.8w}{\beta x u^*}\right) \tag{B.7}$$

where w is the particle settling velocity, b is a constant for a given particle size, *x* is the Von Karman constant, and u* is the friction velocity. Values of b range from 1.0 for fine particles, of 100-mm diameter, to 1.3 for coarse particles, of 0.1mm size. Wasp reported that the Von Karman constant is 0.4 for clear fluid and decreases with particle concentration. In our calculations we used b = 1.0 and *x* = 0.4. The friction velocity is given as

$$u^* = U\sqrt{\frac{f}{2}} \tag{B.8}$$

where U is the bulk flow velocity, and f is the slurry friction factor.

The total pressure drop is the sum of the vehicle friction loss and the friction loss due to the heterogeneity of the remaining solids. The friction factor used for the vehicle portion is found using the Moody diagram, which in the turbulent regime is computed by the following:

$$\frac{1}{\sqrt{f}} = 4\log\frac{D}{2\varepsilon} + 3.48 - 4\log\left(1 + 9.35\frac{D}{2\varepsilon\,Re\sqrt{f}}\right) \tag{B.9}$$

The friction loss comes from the standard relation:

$$\Delta p_{veh} = \frac{h_L}{L} = 4\frac{f}{D}\frac{U_c^2}{2g} \tag{B.10}$$

The "bed friction loss" (Δp_{bed}) is the "overpressure" compared to that of pure water due to the heterogeneity of the remaining solids exclusive of the vehicle and is computed using Durand's equation (Durand 1953):

$$\Delta p_{bed} = 82(\Delta p_{water})C_{v,bed}\left(\frac{gD(s-1)}{U_c^2\sqrt{C_D}}\right)^{1.5} \tag{B.11}$$

Here, Δp_{water} is calculated using Eq. (B.10). Results from Eq. (B.10) and (B.11) have the same dimensions of m/m (or ft/ft). Because the result of (B.10) is in terms of a head of water, the vehicle friction loss must be converted from ft-slurry/ft (m-slurry/m) to ft-water/ft (m-water/m) before adding to the bed pressure drop.

B.4 Calculation Procedure

The vehicle is determined using an iterative mass balance on the vehicle and heterogeneous portions of the solids. Convergence is achieved when the associated pressure drop is unchanging. The computation proceeds as follows:

Step.1. Compute vehicle density, viscosity, pipe Reynolds number, and vehicle friction factor, assuming that all of the solids from each size fraction will enter the vehicle for the first iteration. Friction factor is estimated from Eq. (B.9).

Step. 2. Compute the vehicle friction loss from Eq. (B.10).

Step.3. Also compute clear fluid settling velocities and particle drag for each size fraction.

Step.4. Calculate the friction velocity from Eq. (B.8).

Step.5. Compute the particle settling velocity for each size fraction using vehicle properties.

Step.6. Compute C/C_A for each size fraction from Eq. (B.7).

Step.7. Subtract the fractional vehicle concentrations of each size fraction to obtain the "bed" concentration, assuming that the vehicle part is equal to the product of C/C_A for the size fraction and the volume concentration for that size fraction.

Step.8. Compute Δp_{bed} for each size, using Eq. (B.11), and sum for the bed pressure drop. In the first iteration Δp_{bed} is zero because of the assumption made in Step 1.

Step.9. Sum the fractional vehicle concentrations of each size fraction to obtain the total vehicle concentration.

Step.10. Update the vehicle properties using the vehicle solids concentration.

Step.11. Compute the Reynolds number and find the vehicle friction factor.

Step.12. Calculate the vehicle friction loss from Eq. (B.10).

Step.13. Sum vehicle friction loss and bed pressure drop for the slurry pressure drop.

Step.14. Back out the slurry friction factor, then obtain friction velocity from Eq. (B.10)

Repeat Steps 4-13 until the difference in successive pressure drop calculations is in the third significant digit.

B.5 References

Durand R. 1953. "Basic Relationship of the Transportation of Solids in Pipes – Experimental Research," *Proceedings of Minnesota International Hydraulic Convention*, Minneapolis, MN, pp. 89-103.

Ismail HM. 1952. "Turbulent Transfer Mechanism and Suspended Sediment in Closed Channels," *Trans. ASCE*. Vol. 117, pp. 409-447.

Oroskar AR and RM Turian. 1980. "The Critical Velocity in Pipeline Flow of Slurries." *AIChE Journal*, Vol. 26, No. 4.

Wani CA. 1982. "Critical Velocities in Multisize Particle Transportation Through Horizontal Pipes." *Journal of Pipelines*, Vol. 2, pp. 57-62.

Wasp EJ. 1963. "Cross Country Coal Pipe Line Hydraulics." *Pipeline News*, p. 20.

Wasp EJ. 1977. *Solid-Liquid Flow Slurry Pipeline Transportation*. Trans Tech Publications.

Zandi I and G Govatos. 1967. "Heterogeneous Flow of Solids in Pipelines." *J. Hydr. Div.* ASCE, 93:HY3, Prod. Paper 5244, pp. 145-159.